Title
Novel features of lipase activation revealed by structures of cholesterol esterase

Author
Chen, Julian C.-H.

Publication Date
1999

Peer reviewed|Thesis/dissertation

NOVEL FEATURES OF LIPASE ACTIVATION

REVEALED BY STRUCTURES OF CHOLESTEROL ESTERASE

by

JULIAN C.-H. CHEN

DISSERTATION

Submitted in partial satisfaction of the requirements for the degree of

DOCTOR OF PHILOSOPHY

in

BIOPHYSICS

in the

GRADUATE DIVISION

of the

UNIVERSITY OF CALIFORNIA SAN FRANCISCO

[redacted]

Date **University Librarian**

Degree Conferred: .....

to my family, friends, and teachers

Preface

So this likely is the end of my formal education, a 22 year period of highs, lows, ups and downs, trials, victories, and everything in between. And I have the daunting task of compressing all my thanks onto a couple of pages.

I would like to thank a great number of people in this endeavor known as graduate school, my fellow graduate students Chris Reyes, Sherry LaPorte, Rachel Brem, Bob Keenan, Manish Butte, Russ Huber, Jennifer Harris, Chuck Sindelar, and Kinkead Reiling for being friends and bringing out the lighter, less serious side of me. The Stroud lab was an invaluable resource, especially Paul Foster, Richard Morse, Janet Finer-Moore, Earl Rutenber, Amy Anderson, and Tim Fritz for their help in crystallography and biochemistry and for their patience and time. My closest colleagues on this project were Larry Miercke and Jolanta Krucinski, whose enthusiasm and drive kept the project together and streamlined. Their technical and scientific expertise has been indispensable.

The Molecular Structure Group at UCSF is the finest I've encountered. Help is always nearby and expertise is always sitting next door. My colleagues have been an indispensable resource, Linda Brinen, Andy Shiau, Manish Butte, and Peter Hwang especially, and the members past and present of the Stroud, Fletterick, and Agard labs.

I have kept sane through playing music through my time at UCSF, so I thank Jeremy Swerling for the opportunity to play as soloist with the UCSF Orchestra, Peter Hwang for his dedication to the arts and music at UCSF, and my

Caltech friends Jamie Schlessman, Neill Reid, and Ed and Pam Lewis for many wonderful evenings of music.

Julie Ransom deserves a special thanks for being not only the administrator of the program, but for being a fellow music and opera buff, a wonderful listener, and a great friend. Sherry LaPorte, Chris Reyes, Christa Nunes, and Greg Couch have cultivated my taste for powder and general radness.

And of course this could not be done without the guidance and help of folks from many years past, including Allen Huggett, Jerry Schulmerich, Walter Hellman, Joy Pendergrass, Charles Pease, the late Thor Sabo, and the late Nellie Tholen, who were my best and most influential teachers in my pre-undergraduate years. I thank Douglas Rees, Christof Koch, Robert Sweet, and Venkatraman Ramakrishnan for bringing the excitement and discovery of scientific endeavor to me as an undergraduate at Caltech.

My thesis committee members have been invaluable, Robert Fletterick and Tack Kuntz in particular. Most of all, I thank Robert Stroud, my advisor, mentor, boss, and friend for providing an exciting and knowledgeable lab environment for my graduate work. His optimism and belief in my abilities was unusual and surprising. His scientific sense and deep knowledge of crystallography is contagious, and his encouragement during lean times kept me focused and helped pull me out of those inevitable lows of graduate school.

And finally, I thank my parents and family for their constant, steady support throughout graduate school. I could not manage it without them. So I happily dedicate this work to my family, friends, and teachers.

NOVEL FEATURES OF LIPASE ACTIVATION REVEALED BY STRUCTURES OF CHOLESTEROL ESTERASE

by

Julian C.-H. Chen

ABSTRACT

The lipase cholesterol esterase, also known as bile salt activated lipase, is an important digestive enzyme responsible for hydrolyzing dietary triglycerides and phospholipids, in addition to being the sole enzyme responsible for hydrolyzing dietary cholesterol esters and vitamin esters. Cholesterol esterase is therefore a potential target for lowering plasma cholesterol levels and for the treatment of obesity by inhibition of its esterase properties.

Notable to cholesterol esterase is the dependence of activity on bile salts. The enzyme possesses a basal activity towards water soluble substrates which is enhanced greatly in the presence of bile salts. A double mutant construct of cholesterol esterase designed to remove N-linked glycosylation sites was made and expressed in mammalian cells. The protein was purified, crystallized, and its structure solved to 1.6 Å resolution. The structure reveals an alpha-beta hydrolase fold with a disordered bile salt loop. Notably, the extreme C-terminus of the enzyme lodged in the active site, displacing the oxyanion hole away from a productive binding position and occupying a putative fatty acid binding site.

We proceeded to investigate the bile salt binding properties of cholesterol esterase. We obtained a new crystal form of native bovine cholesterol esterase

with three molecules per asymmetric unit. The new bile salt taurocholate bound and native crystals grow under similar conditions with similar unit cell dimensions. The new apoenzyme structure reveals significant differences among the three monomers as well as from the two apoenzyme structures solved previously. Analysis of these five structures show that domain motions are important in the function of this lipase. We propose that the low basal activity may be due to a mixture of active and inactive catalytic triads.

The structure of the bile salt bound conformation reveals a pre-activated complex. Only one site is occupied appreciably in the taurocholate bound structure, without the second site occupied as seen in the structure of Wang, et al. The molecule appears to 'select' for a competent conformation in which to bind, indicating that the distal site binding stabilizes one of the domains to order the catalytic triad into a productive conformation for substrate binding.

TABLE OF CONTENTS

LIST OF TABLES

Chapter 1. Structure of bovine pancreatic cholesterol esterase at 1.6 Å: novel structural features involved in lipase activation

Chapter 2. The structure of a new crystal form of bile-salt activated lipase highlights biologically relevant domain motions

Chapter 3. The structure of a pre-activated complex of cholesterol esterase with bile salts

LIST OF FIGURES

Chapter 1. Structure of bovine pancreatic cholesterol esterase at 1.6 Å: novel structural features involved in lipase activation.

Chapter 2. The structure of a new crystal form of bile-salt activated lipase highlights biologically relevant domain motions.

Chapter 3. The structure of a pre-activated complex of cholesterol esterase with bile salts.

Introduction

Introduction

Cholesterol esterase, also known as bile salt activated lipase, hydrolyzes a variety of dietary lipids and is the sole enzyme responsible for hydrolyzing dietary cholesterol esters into free cholesterol and fatty acid. This has made it a promising target for inhibitors for use as anti-obesity drugs as well as plasma cholesterol lowering drugs. The enzyme is secreted by the pancreas in large amounts, accounting for approximately 4 % of total protein secreted by the pancreas. Its activity complements that of pancreatic lipase, with substrate targets partially redundant with those of pancreatic lipase. The biological role of cholesterol esterase is significant in early development, in which infants with developing pancreas are given their supply of cholesterol esterase through mother's milk. The presence of this enzyme is correlated with normal development in infants, as lack of the enzyme may stunt development by preventing the complete processing of lipids necessary for growth and brain development. A recent role has been demonstrated for cholesterol esterase in the hepatic uptake of HDL-associated cholesterol esters. Cholesterol esterase binds heparin, likely through a positively charged patch of residues 56-63, and it has been suggested that binding of the enzyme to proteoglycans on the intestinal wall mediates the absorption of free cholesterol. However, a knockout of the cholesterol esterase gene in mice showed no difference in the amount of cholesterol absorbed into the bloodstream.

The hallmark of the enzyme is its lipolytic activity that is dependent on bile salts for optimal activity. Bile salts are polar derivatives of cholesterol,

secreted through the bile duct into the small intestine. Bile salts, because of their amphipathic properties, act as emulsifiers for the dietary lipids ingested as food. It also plays a functional role in the enzyme by binding to the protein through two sites.

The protein itself is highly conserved throughout the species, with a central core of about 535 amino acids and a tail region of proline-rich repeats of 11 amino acids per repeat, with a consensus sequence of $(PVPPTGDSGAP)_n$. The number of repeats are the significant difference in cholesterol esterase across the species and account for the different molecular weights of cholesterol esterase. Bovine pancreatic cholesterol esterase is 579 amino acids, containing three repeats, while human pancreatic cholesterol esterase is 722 amino acids long, with 16 such repeats. The core region of cholesterol esterase shares about 31 % sequence identity with acetylcholinesterase from *Torpedo californica*. An additional 24 % of residues are conservative substitutions. This sequence identity implied a structural similarity between the enzymes. This and biochemical studies highlighted a catalytic triad of a serine, histidine, and aspartic acid, similar to those from the serine proteases.

I have attempted to better define the structural transitions between a non-activated, apoenzyme form of cholesterol esterase and the bile salt bound, activated form of the enzyme through crystallographic studies. In the context of understanding lipases, the studies presented here in addition to the structure of Wang, et al. have increased our understanding of the process of activation of cholesterol esterase by bile salts. The enzyme is also a drug target, with an anti-obesity drug recently marketed by Wyeth-Ayerst. As it is becoming more evident that structure-based drug design must take into account the dynamics of the

protein, the structures here present a dynamical view of cholesterol esterase. These structures shed light on the solution properties and conformational flexibility of cholesterol esterase and aid further design of inhibitors against the enzyme.

Chapter 1 describes the high resolution structure of a recombinant form of cholesterol esterase. The impetus behind this construct was to remove heterogeneities from the two N-linked glycosylation sites on the enzyme. This was done by mutations of Asn 187 and Asn 361 to Gln. The resulting enzyme was biochemically characterized and found to be identical to the wild-type, glycosylated enzyme. Crystals of this mutant enzyme were grown, and the structure was solved to 1.6 Å resolution. Notably, the bile salt loop is disordered in the structure, but surprisingly, the extreme C terminus of the enzyme is lodged in the active site, occupying the putative fatty acid binding pocket. These features are unique in lipases, and identify a previously unknown role for the C terminal region of the enzyme, which can be thought of as a tethered plug. Furthermore, these novel features suggest a different set of conformational rearrangements upon bile salt activation compared to the triglyceride lipases.

Due to our inability of obtain suitable crystals of the taurocholate/cholesterol esterase complex using our mutant protein, we returned to the native enzyme from bovine pancreas and obtained a new crystal form of the enzyme. Chapter 2 describes this work. In summary, this new crystal form reveals several intriguing features, notably that the enzyme adopts a wider variety of conformations than other triglyceride lipases, perhaps reflective of its promiscuous substrate specificity. It also suggests a role for bile salt binding, not

only in activating the enzyme, but by stabilizing the catalytic triad in a productive orientation for hydrolysis.

In an attempt to crystallize the taurocholate/cholesterol esterase complex in this new condition, we were unable to see the binding of bile salt to the activating bile salt loop. However, we see bile salt bound to a cleft between the domain containing the active site triad and a helical region nearby. A structure in the presence of the non-activating bile salt taurodeoxycholate, lacking the 7-α hydroxyl group of taurocholate, shows the bile salt bound in the same location and in a similar orientation. We have therefore located a nonspecific bile salt binding site. As electron density for bile salt is clearly seen in only one monomer of the three in the asymmetric unit, we propose that the bile salt binding in the region may select for a particular conformation, or stabilize the ensemble of accessible conformations to one that is catalytically competent. In essence we have captured the enzyme in a pre-activated state.

Chapter 1

Structure of bovine pancreatic cholesterol esterase at 1.6 Å: novel structural features involved in lipase activation

published in Biochemistry, 37(15), 5107-5117, 1998.

Structure of bovine pancreatic cholesterol esterase at 1.6 Å: novel structural features involved in lipase activation†

†This work was supported by grants from the NIH GM24485 (R.M.S.)

Julian C.-H. Chen, Larry J.W. Miercke‡, Jolanta Krucinski‡, Jacqueline R. Starr§||, Gina Saenz§^, Xingbo Wang§, Curtis A. Spilburg§#, Louis G. Lange§, Jeff L. Ellsworth§%, and Robert M. Stroud*‡

Graduate Group in Biophysics and ‡Department of Biochemistry and Biophysics, University of California, San Francisco, CA 94143, and §CV Therapeutics, Inc., 3172 Porter Drive, Palo Alto, CA 94306.

||Present address: Department of Epidemiology, Box 357236, University of Washington, Seattle, WA 98195-7236.

^Present address: Dade Behring, MicroScan, 2040 Enterprise Boulevard, West Sacramento, CA 95691.

#Present address: Department of Medicine, Cardiology Division, Jewish Hospital of St. Louis, Washington University Medical Center, St. Louis, MO 63310.

%Present address: ZymoGenetics, Inc., 1201 Eastlake Avenue East, Seattle, WA 98102.

Running Title: 1.6 Å Structure of Pancreatic Cholesterol Esterase

Coordinates have been deposited in the PDB with accession number 2bce and will be available within a year of publication of this manuscript.

ABBREVIATIONS AND TEXTUAL FOOTNOTES

CEase, cholesterol esterase

CEase-C, cholesterol esterase with amino acids 574-579 deleted

PC, phosphatidylcholine

TC, taurocholate

p-NPB, p-nitrophenyl butyrate

HEK, human embryonic kidney

HDL, high density lipoprotein

SDS-PAGE, sodium dodecyl sulfate polyacrylamide gel electrophoresis

IEF, isoelectric focusing

DLS, dynamic light scattering

MES, 2-(*N*-morpholino)ethanesulfonic acid

HEPES, *N*-2-hydroxyethylpiperazine-*N'*-2-ethanesulfonic acid

CHES, 2-(*N*-cyclohexylamino)ethanesulfonic acid

ABSTRACT

The structure of pancreatic cholesterol esterase, an enzyme that hydrolyzes a wide variety of dietary lipids, mediates the absorption of cholesterol esters, and is dependent on bile salts for optimal activity, is determined to 1.6 Å resolution. A full length construct, mutated to eliminate two N-linked glycosylation sites (N187Q,N361Q), was expressed in HEK 293 cells. Enzymatic activity assays show that the purified, recombinant, mutant enzyme has identical activity to the native, glycosylated enzyme purified from bovine pancreas. The mutant enzyme is monomeric and exhibits improved homogeneity which aided in the growth of well-diffracting crystals. Crystals of the mutant enzyme grew in space group *C*2, with *a*= 100.42 Å, *b*= 54.25 Å, *c*= 106.34 Å, β= 104.12, with a monomer in the asymmetric unit. The high resolution crystal structure of bovine pancreatic cholesterol esterase (R_{cryst} = 21.1 %; R_{free} = 25.0 % to 1.6 Å resolution) shows an alpha-beta hydrolase fold with an unusual active site environment around the catalytic triad. The hydrophobic C-terminus of the protein is lodged in the active site, diverting the oxyanion hole away from the productive binding site and the catalytic Ser 194. The amphipathic, helical lid found in other triglyceride lipases is truncated in the structure of cholesterol esterase and therefore is not a salient feature of activation of this lipase. These two structural features, along with the bile salt dependent activity of the enzyme, implicate a new mode of lipase activation.

Pancreatic cholesterol esterase (CEase), also known as bile salt activated lipase, is responsible for the hydrolysis of dietary cholesterol esters, fat soluble vitamin esters, phospholipids, and triglycerides (1, 2). As such, it is one of the central enzymes that mediates absorption of dietary lipids through the intestinal wall into the bloodstream. A number of studies have suggested a possible role for CEase in the absorption of free cholesterol at the brush border membrane of the small intestine (3-6), though a CEase gene knockout showed little change in the absorption of cholesterol (7). CEase is present in high concentrations in breast milk and plays a crucial role in development by supplying the enzyme to infants whose pancreas are not yet fully developed (1, 2). A role has also been demonstrated for CEase in the hepatic uptake of HDL-associated cholesterol esters (8). The bile salt dependence of enzymatic activity identifies CEase as a distinct lipase with necessarily different structural changes upon activation.

Bovine pancreatic CEase is a glycoprotein of 579 amino acids, with a notable proline-rich region between amino acids 540 and 573, and a highly conserved six amino acid hydrophobic sequence forming the extreme C-terminus of the protein (9). The proline-rich region is composed of a consensus repeat sequence of $(PVPPTGDSGAP)_n$, and the number of repeats marks the major difference between CEases across the species (2); bovine pancreatic CEase contains three such repeats, while human CEase contains sixteen repeats. Studies of the proline-rich repeats show no role in enzymatic activity, and a physiological role for this region remains elusive (10-13). The proline-rich repeats are also serine and threonine rich and contain putative sites for O-glycosylation. There are also two sites for N-linked glycosylation at residues 187 and 361 (9, 14).

The purpose of this study was to determine the high resolution crystal structure of bovine pancreatic CEase to gain insight into the molecular recognition of sterols, the mechanisms of cholesterol absorption, sites of interaction with bile salt, and the mechanism of activation of this distinct lipase. Since high resolution diffraction quality crystals could not be initially obtained from native wild-type protein (C.A. Spilburg and L.G. Lange, unpublished), the two N-linked sugars were removed by mutating asparagines 187 and 361 in the N-linked glycosylation consensus sequences to glutamines, followed by overexpression in HEK 293 cells. The purified double mutant CEase was evaluated for electrophoretic purity (SDS-PAGE, native PAGE, and IEF), functional activity by cholesteryl oleate hydrolysis and p-nitrophenyl butyrate (p-NPB) hydrolysis, and oligomeric state and homogeneity by dynamic light scattering (DLS).

As this paper was being submitted, the 2.8 Å structure of the native enzyme alone and in complex with bile salt was solved independently, in a different space group (15). Interestingly, their apoenzyme structure is in a different conformation than our apoenzyme structure at 1.6 Å resolution, which suggests a role for the aliphatic chain of the fatty acid, mimicked by detergent in their structure, and a critical role for the C-terminus in the activation of the lipase revealed in ours (16). Our structure shows a clear biological role for the C-terminal region of the enzyme and implicates novel structural features in the activation of this lipase.

MATERIALS AND METHODS

Cloning, Mutagenesis, and Expression. Bovine pancreatic CEase was cloned as previously described (9). The full length, double mutant CEase was constructed by first creating two single mutants, N187Q and N361Q, using PCR-based mutagenesis (17). N187Q was created using the mutagenic oligonucleotide 5'-GGAGACCCCGACCAAATCACCCTCTTTG-3', while N361Q used the oligonucleotide 5'-CTCAGAGGTGCCGACGCCACGTACGAG-3'. The two cloned inserts were sequenced, then cleaved with restriction enzyme *Cla*I, located between the codons for amino acids 187 and 361. The 5' portion of N187Q and the 3' portion of N361Q were then ligated together into a pCEP4 expression vector (Invitrogen) and expressed in HEK 293 cells as described previously (18) .

Purification of native and mutant CEases. Native CEase from bovine pancreas and double mutant N187Q,N361Q CEase expressed in HEK 293 cells were purified as previously described (18), with the double mutant CEase requiring modifications. For the double mutant, 2.1 L cell media was adjusted to 20 mM MES 6.0 with 1.0 M MES, 0.45 μm filtered, and CEase precipitated by addition of ammonium sulfate (856 g to 2.1 L) with stirring for 3 hr. The pellet was resuspended in 100 mL 20 mM MES 6.0 and dialyzed against 20 mM MES 6.0. Following S-sepharose chromatography (3 cm x 40 cm; equilibrated and loaded with 20 mM MES pH 6.0, washed with 0.15 M NaCl, and CEase eluted at 0.2 to 0.35 M NaCl using a 0.15 M to 0.6M NaCl gradient), p-nitrophenyl butyrate (p-NPB; Sigma) active fractions were pooled, concentrated to approximately 10 ml, and dialyzed for 24 hr against 100 mM MES 6.0. The sample was applied to a

1.2 cm x 10 cm Poros CM weak cation exchanger (Perseptive Biosystems) run at 3 ml/min in 100 mM MES pH 6.0 with 2 ml injection loads. CEase was retarded on the column with elution post flow through at 1.5 to 4.5 min. At 5 min post injection, a 3.5 min 0 M to 0.7 M NaCl gradient was run to remove impurities followed by 5 min re-equilibration. Pooled CEase was concentrated to approximately 5 ml and dialyzed against the appropriate buffer. Protein was concentrated by high-pressure stirred cell ultrafiltration using YM-10 membranes (Amicon). Protein concentration was determined by the Bradford method using bovine serum albumin as a standard.

Electrophoretic and molecular size characterization. SDS-PAGE and native PAGE were performed using a Novex Xcell II Mini Cell and 4-20% acrylamide/Tris-glycine precast gels in the presence and absence of 0.1 % SDS in the running buffer. Samples were prepared by mixing with an equal volume of 2X reducing application buffer (SDS-PAGE) or running buffer (native PAGE). Isoelectric focusing (IEF) was performed using precast pH 3-10 ampholite gels. IEF samples were diluted with equal volumes of IEF sample buffer. Gels were run according to Novex Precast Gel Instructions. Molecular weight and oligomeric state were assayed using the DynoPro-801 Dynamic Light Scattering Instrument equipped with a micro-cuvette based MicroSampler (Protein Solutions). Prior to data collection, 1.2 mg/ml protein in 10 mM MES 6.0 was filtered through a 0.02 µm Anodisc membrane using the MicroFilter system (Protein Solutions). Software version 3.00 was used for instrument control and data collection.

Enzymatic activity assays. Functional activity of both native and mutant CEases were assayed by monitoring the hydrolysis of cholesteryl oleate and p-

NPB as a function of pH, enzyme concentration, and taurocholate (TC; Sigma) concentration. [1-^{14}C] Oleic acid release after a 5 minute incubation period at 37 C from vesicles containing cholesteryl [1-^{14}C] oleate (Amersham) and egg yolk phosphatidylcholine (PC; Sigma) was measured as previously described (19). Samples (25 ng CEase/275 µl) were prepared by mixing 175 µl of 100 mM buffer (sodium acetate pH 4.0 and 5.0, MES pH 6.0, HEPES pH 7.0, Tris pH 8.0, CHES pH 9.0), 75 µl cholesteryl [1-^{14}C] oleate vesicles in 2.0 mM Tris pH 7.2, ≤ 5.5 µl 500 mM TC, 20 µl CEase diluted 1000 fold in the appropriate pH buffer, and water to give a total volume of 275 µl. The rate of p-NPB hydrolysis at 25 C was determined from the linear portion of the absorbance curve (10 to 70 sec) at 405 nm using a Shimadzu UV-160 spectrophotometer equipped with a liquid temperature control system. CEase in 10 mM MES pH 6.0 was diluted 50 fold in buffer (same as above) containing the appropriate TC concentration to give 0.02 mg/ml CEase. p-NPB was prepared by mixing 250 µl fresh stock (9 µl in 1 ml dioxane) into 25 ml 25 mM MES, pH 6.0. The reaction was initiated by addition of 2 µl p-NPB to 1 ml protein solution directly in a quartz cuvette.

Crystallization and data collection. For crystallization, purified N187Q,N361Q CEase was dialyzed against 2 mM sodium phosphate pH 7.0 and further concentrated to 5-6 mg/ml. Crystals were grown at room temperature in hanging drops by mixing equal volumes of protein with well buffer containing 0.1 M sodium acetate pH 4.5, 1.5 M ammonium sulfate, and 6 % isopropanol. Crystals appeared in 5-8 days as twinned clusters of thin rods, averaging 200 µm x 60 µm x 30 µm in size, with a small number of single, untwinned crystals suitable for data collection. Data were collected on a 30 cm image plate (MAR

Research). Cryoprotectant of mother liquor containing 30 % glycerol was applied to the crystal shortly before flash freezing in a 90 K nitrogen gas stream. A complete dataset was collected on a single frozen crystal at Stanford Synchotron Radiation Laboratory beamline 7-1 (λ = 1.08 Å), with diffraction observed to the edge of the image plate at 1.6 Å resolution. Data were indexed, integrated, and scaled using DENZO and SCALEPACK with no sigma cutoff, indexing in space group C2, a= 100.42 Å, b= 54.25 Å, c= 106.34 Å, β= 104.12, with a monomer in the asymmetric unit. A summary of data collection and refinement statistics is presented in Table 1.

Crystallography and structure refinement. Molecular replacement in AMoRe (20) was used to generate an initial map, and the model was improved by cycles of manual building in CHAIN (21) and refinement in XPLOR (22). Briefly, the primary sequences of bovine pancreatic CEase and *Torpedo californica* acetylcholinesterase were aligned, and the acetylcholinesterase coordinates (PDB code 2ace) truncated to a discontinuous, 368 amino acid core corresponding to conserved regions of sequence and secondary structure (23). Rotation and translation searches, followed by rigid-body refinement in AMoRe yielded an unambiguous solution and a starting R_{cryst} of 48.3 %. A 7.0 % set of reflections was set aside for calculation of R_{free} prior to refinement in XPLOR (24). An immediate bulk solvent correction followed by simulated annealing refinement reduced the R_{cryst} to 44.3 %, with clear density corresponding to the primary sequence of CEase. Manual rebuilding followed by cycles of conjugate gradient minimization, simulated annealing, and temperature factor refinement (40 - 1.6 Å) dropped the R_{cryst} and R_{free} to 21.1 and 25.0 %, respectively. A bulk solvent

correction was applied regularly throughout refinement. MIDAS was used for docking the cholesterol ester (25). Ramachandran parameters were monitored using PROCHECK (26).

RESULTS

Protein Expression, Purification and Characterization. The three step purification procedure produced 5-7 mgs of purified, recombinant double mutant from 2.1 L expression media. The purified N187Q,N361Q mutant CEase consists of one SDS-PAGE band, one native PAGE band, and 3 IEF bands with pI's between 4.8 and 4.9 (Figure 1). In comparison, native CEase purified from bovine pancreas migrates as a single, slightly faster migrating SDS-PAGE band, a smeared, impeded multi-banded pattern on native PAGE, and multiple IEF bands with pI's between 4.9 and 5.1 (Figure 1). These three electrophoretic assays are indicative of glycosylation in native CEase.

Both the mutant N187Q,N361Q and native CEases exhibit essentially identical functional activity (Figure 2). Both enzymes show similar cholesteryl [1-^{14}C] oleate hydrolytic activities as a function of enzyme concentration (Figure 2a), with peak hydrolytic activity at pH 7.0 (Figure 2b). Both enzymes show similar bile salt taurocholate (TC) dependence of enzymatic activity, with half-maximal activity around 5.0 mM TC (Figure 2c). Using the water soluble ester p-NPB, both enzymes display similar profiles as a function of pH and TC concentration, with half-maximal activity at ~0.4 mM TC, pH 7.0 (Figure 2d).

Taken together, these experiments show that the presence of the N-linked sugars is not required for ester hydrolysis.

Further characterization of the purified mutant CEase by DLS yields a sample with a narrow, monomodal distribution (baseline of 0.999-1.000) of monomers, with a molecular weight of 61.2 ± 1.2 kD and 65.5 ± 1.5 kD, based on two independent samples of 14 and 20 measurements, respectively. This is in agreement with the calculated 63.5 kD molecular weight of the mutant, unglycosylated enzyme. In addition, characterization of native bovine CEase also shows a homogeneous, monomodal distribution of the monomer, with an average molecular weight of 64.0 ± 3.0 kD.

Crystal Structure. The structure was solved by molecular replacement based on a truncated model of *Torpedo californica* acetylcholinesterase (Table 1) (23). CEase is a member of the alpha-beta hydrolase superfamily, the general fold found in esterases and other triglyceride lipase structures, typically fungal. The structure is composed of a system of eleven beta strands forming the core of the protein surrounded by fifteen alpha helices (Figure 3), with very clear electron density throughout the molecule (Figure 4). The catalytic triad of Asp 320, His 435, and Ser 194 is located roughly at the center of the molecule. The unique environment around the active site residues distinguishes pancreatic CEase from other lipases (Figure 5). Based on homology to residues in acetylcholinesterase, Ala 195, Gly 107, and Ala 108 of CEase are likely involved in coordinating the oxyanion intermediate in the reaction. Ala 195 forms the N-terminus of a 11 residue alpha helix, placing it at the positive end of the helix dipole, contributing to the stabilization of the negatively charged reaction intermediate (27). A water molecule hydrogen bonds to the amino group of Ala 195 in the apoenzyme

structure. Strikingly, the extreme C-terminus with its hydrophobic sequence PVVIGF is lodged in the active site (Figures 5, 6a). The C-terminus physically displaces the putative oxyanion binding residues Gly 107 and Ala 108 away from the catalytic serine. Compared to acetylcholinesterase, the side chain of conserved Tyr 105 is flipped, and the residues following veer away from the active site (Figure 6a). The hydrophobic C-terminus also functions as a plug, and a calculation of accessible surface area upon removal of this hexapeptide shows that 37 mostly hydrophobic residues and 504 $Å^2$ of surface area are exposed. Importantly, the catalytic serine and histidine, and the putative oxyanion binding residues are made more accessible to substrate (Table 2). Therefore this C-terminal hexapeptide clearly plays a role in the lipase activation pathway of this enzyme.

CEase also lacks an amphipathic, helical lid region important for interfacial activation found in triglyceride lipases, and instead, it is truncated into a pair of antiparallel beta strands. The N-terminal disulfide loop in CEase, containing residues 64 to 80, makes up this truncated lid region. A superposition of the structures of pancreatic CEase and *Candida cylindracea* CEase (28) clearly shows the truncation of the lid region (Figure 6b).

There are three distinct systems of beta sheets, two core systems conserved in the alpha-beta hydrolase fold, and a unique third system lying near the active site. This third set of beta sheets is composed of four strands, amino acids 66 to 68 and 74 to 76 in the truncated lid region, amino acids 108 to 110, and amino acids 575 to 577 in the extreme C-terminus (Figure 3). Immediately preceding the extreme C-terminus is a proline-rich repeat region, composed of

the consensus repeat sequence $(PVPPTGDSGAP)_n$, where n ranges from 3 in bovine to 16 in human (2). This proline-rich repeat is disordered in the electron density and presumably very flexible.

Residues 113-119 in CEase are also disordered in the electron density, corresponding to a hydrophilic loop near the active site that is conserved in all CEase sequences, but absent in other lipases and esterases. This was earlier proposed to be a bile salt binding site, and was found to be similarly disordered in the 2.8 Å apoenzyme structure (15).

An electrostatic potential map of the protein surface reveals unusually large patches of negative potential, with a small number of neutral and positive potential areas (Figure 7a). A conglomerate of positive charge is centered around residues 56-63, which was earlier determined to be the site of interaction with heparin-like molecules on the cell surface (29) (Figure 3). The primary sequence in this region, KAKSFKKR, is similar to other heparin binding sequences (2, 29) This patch is located 17-30 Å away from the catalytic Ser 194, consistent with its proposed role of anchoring to the cell surface (4-6).

A large lobe of negative potential lies proximal to the active site, in a helical domain composed of residues 322 to 376. In addition to this segregated distribution of charge, CEase also has an unusual distribution of temperature factors (Figure 7b). CEase shows a patch of systematically higher temperature factors also located in helical domain containing residues 322 to 376. This region of higher temperature factors is strikingly coincident with the area of negative potential, suggesting a possible role for electrostatic interactions between the mixed micelle and the enzyme.

DISCUSSION

Purification and characterization of CEase. The mutation of the two N-linked glycosylation sites and the subsequent expression, purification, and functional characterization shows that no N-linked oligosaccharides are involved in the hydrolytic activity of the enzyme. Electrophoretic characterization of native CEase shows that the increase in the number of isoelectric forms and average pI relative to mutant CEase, and the change in mass to charge ratio in native CEase is due to the presence of the N-linked sugars. Even though the function of the N-linked sugars is not well understood, rat pancreatic CEase lacking the N-linked sugars was secreted at 50 % lower levels in Chinese hamster ovary and pancreatoma cells, showing a role for glycosylation in the secretion of the enzyme *in vivo* (30, 31). The N-linked sugars are also implicated in protein folding and thermal stability of the enzyme (31). Although the amino acids in the region surrounding residues 187 and 361 are neutral to hydrophilic, the N-linked sugars may also play a role in improved solubility. We show by DLS and crystal packing that bovine CEase is a functional monomer as is human CEase (32). Therefore the native CEase dimers, present in both the uncomplexed and TC complexed structures of Wang, et al. are due to crystallization conditions and crystal packing. Crucial to this study was the increased homogeneity in the double mutant. Previously, we were unable to obtain atomic resolution data from native CEase crystals, and the improvements in homogeneity brought

about by the removal of the N-linked sugars may have contributed to the growth of well ordered crystals.

A possible role for the C-terminus in lipase activation. The structure of CEase at 1.6 Å resolution shows an alpha-beta hydrolase with an unusual active site region, where the last six amino acids of the enzyme, PVVIGF, splay the putative oxyanion hole away from the active site (Figure 5, 6a). Defining a biological role for the C-terminus has been difficult (13); however, the last six amino acids are highly conserved among mammalian CEases (Table 3). Therefore, we expect that the C-terminus plays a similar role in the function of these enzymes. The length of the proline-rich repeats preceding the C-terminus varies across the mammalian CEases, with three repeats in the bovine enzyme, four in the rat enzyme, and sixteen in the human enzyme. Structurally, the proline-rich repeats act as a tether to the C-terminus and may exhibit similar disorder in the structures of other mammalian CEases.

The removal of the final six amino acids (CEase-C) exposes a predominantly hydrophobic 504 $Å^2$ of surface area (Table 2). Manual docking of cholesteryl linoleate (PDB code 1cle) into the active site of CEase-C indicates that the alkyl chain of the fatty acid fits in the hydrophobic pocket left by the removal of the terminal amino acids, with the proper tetrahedral geometry dictated by the oxyanion intermediate (Figures 8,9) (28). Given that this probable binding mode of the cholesteryl ester occupies the same hydrophobic pocket as the C-terminus, we propose that the C-terminal peptide must move in order to accommodate the substrate. The structure shows that this hexapeptide plays an important role in the function of this enzyme not only by the displacement of the oxyanion hole

away from the active site, but also by occupying a deep hydrophobic pocket that is of a size to accommodate the fatty acid of a cholesterol ester (Figure 8).

The truncation of the lid region in pancreatic CEase and the presence of the C-terminal peptide in the active site suggest a unique set of structural rearrangements required for lipase activation. Whether the movement of the peptide is driven by substrate, by bile salt, or by a combination of the two, is unclear. The movement of the C-terminal peptide may be driven by the interaction with bile salt. As the C-terminal residues are hydrogen bonded to the mobile loop implicated in bile salt activation, binding of bile salt and the subsequent ordering of residues 113-119 may contribute to the movement of the C-terminal peptide (33). Furthermore, enzymatic data on native and truncated forms of CEase, where the proline-rich repeats and the hydrophobic C-terminus were deleted, show that the truncated and native CEases are kinetically indistinguishable in the presence of saturating concentrations of bile salt, and are therefore structurally indistinguishable, indicative of a displaced C-terminus in the presence of bile salt (33). Therefore as the enzyme binds to the bile salt, the resulting displacement of the C-terminus allows the loop containing the oxyanion binding site to move into a position that can coordinate the intermediate (Figures 5, 6a).

The movement of the C-terminal peptide may also be driven by substrate binding, as implicated by the crystal structure of the apoenzyme of CEase in the presence of detergent. Wang, et al., in their structure of the apoenzyme determined independently at 2.8 Å resolution, show a preformed oxyanion hole with no density seen for the C-terminus. While our construct involved mutation of two N-linked consensus glycosylation sequences, the differences in the

apoenzyme structures are not due to the lack of N-linked glycosylation in our structure. The N-linked glycosylation sties are distal to the active site and C terminus, and furthermore, activity assays on the native and mutant CEases show identical enzymatic activity (Figure 2); therefore, glycosylation does not play a role in the conformational differences between our structure and that of Wang, et al. In light of their structure, it appears that crystallization conditions may account for the notable differences between their apoenzyme structure and ours. The authors use the detergent zwittergent 3-12 as an additive in the crystallization. Despite the lack of detergent density in the putative fatty acid binding pocket, it is possible that the long alkyl chain of the detergent may have helped displace the C-terminus from the active site, allowing the oxyanion hole to move into its productive binding position. This is consistent with the known sensitivity of the conformation of lipase structures to crystallization conditions and suggests a role for substrate in the displacement of the C-terminus. Our crystals lack any detergent and therefore may more accurately reflect the conformation of the enzyme in the absence of bile salt. Nevertheless, the enzymatic data and the crystal structure of the apoenzyme in the presence of detergent coupled with our high-resolution apoenzyme structure point toward a clear role for the displacement of the C-terminus during lipase activation.

Bile salt binding and enzymatic activity. Characterization of native and mutant CEases shows different bile salt concentration dependence curves of enzymatic activity for water soluble vs. hydrophobic esters, with an observed half-maximal activation for TC around 400 μM in the case of water soluble ester hydrolysis, and half-maximal activation at a TC concentration of 5.0 mM in the case of cholesteryl oleate hydrolysis. While these numbers cannot be directly

compared due to the unknown concentration of substrate in the micelle and the dynamic physical chemical properties of the mixed micelle, 5.0 mM is in the range of the critical micelle concentration of TC, suggesting a role of TC as a surfactant in addition to being an activator of CEase. From the independently determined 2.8 Å structure of the enzyme complexed with bile salt, two binding sites were found, a proximal site and a distal site. The proximal site near the catalytic triad orders residues 116-125 and swings the binding loop away from the active site, thus allowing easier access of substrate (15). Based on our apoenzyme structure, we argue that the second, distal site may be involved in opening the substrate binding pocket to accommodate the bulkier cholesterol esters. The distal bile salt binding site is located in a cleft between the helical bundle domain of residues 322-376 and the core of the enzyme. This is consistent with the temperature factor distribution of our structure, where this same helical bundle domain has systematically higher temperature factors than the remainder of the molecule (Figure 7b). This domain may be ordered by the binding of bile salt to the distal site.

An electrostatic role in lipase activation? Pancreatic CEase shows a patch of systematically higher temperature factors located in the helical domain containing residues 322 to 376 (Figure 7b), coincident with the area of negative potential (Figure 7a). Because of the charged nature of the more mobile regions of the molecule, we propose a role for electrostatic interactions in binding the mixed micelle. Interactions of CEase with mixed micelles of bile salt and phospholipids, containing free cholesterol, cholesterol esters, and triglycerides may be mediated by the positive charge on phospholipids such as phosphatidylcholine. As the phospholipids and cholesterol esters are

hydrolyzed, changes to the physical chemical properties of the mixed micelle lead to dissociation from the protein. This region may thus have evolved to properly orient the enzyme face relative to the mixed micelle.

Evolutionary aspects. Though evolutionarily unrelated, the mechanism of hydrolysis by CEase has profound homology to the mechanisms of hydrolysis of esters by the serine proteases. Therefore the comparisons of the active site structures provide another critical assessment of the features most important to the chemical mechanisms of hydrolysis. The docking of cholesteryl linoleate into the active center allows for an assessment of contributions that may pertain to the mechanism of hydrolysis (Figure 8). From this model the ester bond can be brought against the γO of Ser 194 and the εN of His 435 in a manner that suggests the stereochemistry of nucleophilic attack by the γO of Ser 194 on the carbonyl carbon of the ester. This model predicts that the nucleophilic attack takes place from the opposite side of the ester, leading to the inversion of chirality of the tetrahedral intermediate with respect to the trypsin-like serine proteases (Figure 9). This predicted stereochemical inversion is consistent with the structures of other triglyceride lipases in complex with inhibitors (34-37). From our docking, the hydrogen bonds from the imidazole to the γO of Ser 194 and from the Nδ2 of His 435 to the γO of Asp 320 are essentially coplanar, making excellent hydrogen bonded geometry between them. The geometry of the catalytic triad is ideally suited for the εN of His 435 to act first as a base for the serine proton, then as an acid to the oxygen of the cholesterol leaving group, presenting both oxygens in a coplanar manner with the plane of the imidazole. An additional similarity is the doubly hydrogen bonded support by two donors to the other oxygen of Asp 320.

These have direct analogs in the serine proteases, however this oxygen lies in the opposite relative orientation with respect to the imidazole in the proteases. The oxyanion in the tetrahedral intermediate can be readily stabilized by the NH of Ala 195, however, a second hydrogen bond would require the active site to close over the substrate. A primary candidate for a second bond is the NH of Gly 107, once oriented in the correct direction.

CEase hydrolyzes both water soluble and hydrophobic esters, and its structure places it evolutionarily between the triglyceride lipases and the esterases. The triglyceride lipases preferentially hydrolyze hydrophobic esters and lipids while esterases such as acetylcholinesterase function mainly on water-soluble substrates. For CEase to accommodate larger, more hydrophobic esters, bile salt is required, in a dual role as a molecule binding specifically to CEase to open the active site to these bulkier molecules, and as a surfactant to solubilize the hydrophobic esters, phospholipids, and triglycerides. Therefore, the bile salt dependence of CEase allows the enzyme to accommodate both hydrophilic and hydrophobic substrates.

The structure of CEase suggests a unique mode of lipase activation. To date, most triglyceride lipase structures are distinguished by a amphipathic, helical lid covering the active site catalytic triad, shielding the hydrophobic binding pocket from substrate (35, 38). During interfacial activation, the helical lid swings open upon contact with the hydrophobic substrate, revealing a binding pocket readily accessible to substrate. There is no amphipathic lid in the structure of CEase, rather, a broader rearrangement of the tertiary structure is necessary for its physiological activity, mediated by bile salt and substrate

binding. The displacement of the C-terminus lodged in the active site is also necessary for substrate binding, as this reveals the hydrophobic binding site for the acid portion of the ester and allows the oxyanion hole to form properly to bind the reaction intermediate. Furthermore, the bile salt dependence of enzymatic activity coupled with these unusual structural features distinguish CEase as a novel lipase with an unusual mode of lipase activation.

ACKNOWLEDGMENT

We thank S.L. LaPorte and Dr. Janet Finer-Moore for critical comments on the manuscript, and Drs. Finer-Moore and Earl Rutenber for assistance with the structure refinement.

REFERENCES

1. Hui, D. Y. (1996) *Biochem. Biophys. Acta 1303*, 1-14.

2. Wang, C. S., & Hartsuck, J. A. (1993) *Biochem. Biophys. Acta 1166*, 1-19.

3. Mackay, K., Starr, J. R., Lawn, R. M., & Ellsworth, J. L. (1997) *J. Biol. Chem. 272*, 13380-13389.

4. Lopez-Candales, A., Bosner, M. S., Spilburg, C. A., & Lange, L. G. (1993) *Biochemistry 32*, 12085-9.

5. Bosner, M. S., Gulick, T., Riley, D. J. S., Spilburg, C. A., & Lange, L. G. (1988) *Proc. Natl. Acad. Sci. U S A 85*, 7438-42.

6. Bosner, M. S., Gulick, T., Riley, D. J. S., Spilburg, C. A., & Lange, L. G. (1989) *J. Biol. Chem. 264*, 20261-4.

7. Howles, P. N., Carter, C. P., & Hui, D. Y. (1996) *J Biol. Chem. 271*, 7196-202.

8. Li, F., Huang, Y., & Hui, D. Y. (1996) *Biochemistry 35*, 6657-63.

9. Kyger, E. M., Wiegand, R. C., & Lange, L. G. (1989) *Biochem. Biophys. Res. Commun. 164*, 1302-9.

10. Wang, C. S., Dashti, A., Jackson, K. W., Yeh, J. C., Cummings, R. D., & Tang, J. (1995) *Biochemistry 34*, 10639-44.

11. Hansson, L., Blackberg, L., Edlund, M., Lundberg, L., Stromqvist, M., & Hernell, O. (1993) *J. Biol. Chem. 268*, 26692-26698.

12. Blackberg, L., Stromqvist, M., Edlund, M., Juneblad, K., Lundberg, L., Hansson, L., & Hernell, O. (1995) *Eur. J. Biochem. 228*, 817-821.

13. Downs, D., Xu, Y. Y., Tang, J., & Wang, C. S. (1994) *Biochemistry 33*, 7979-85.

14. Sugo, T., Mas, E., Abouakil, N., Endo, T., Escribano, M.-J., Kobata, A., & Lombardo, D. (1993) *Eur. J. Biochem. 216*, 799-805.

15. Wang, X., Wang, C.-S., Tang, J., Dyda, F., & Zhang, X. C. (1997) *Structure 5*, 1209-1218.

16. Chen, J. C.-H., Miercke, L. J. W., Krucinski, J., Starr, J. R., Saenz, G., Wang, X., Spilburg, C. A., Lange, L. G., Ellsworth, J. L., & Stroud, R. M. (1997) *FASEB J. 11*, A1064.

17. Good, L., & Nazar, R. N. (1992) *Nucleic Acids Res. 20*, 4934.

18. Spilburg, C. A., Cox, D. G., Wang, X., Bernat, B. A., Bosner, M. S., & Lange, L. G. (1995) *Biochemistry 34*, 15532-8.

19. Cox, D. G., Leung, C. K., Kyger, E. M., Spilburg, C. A., & Lange, L. G. (1990) *Biochemistry 29*, 3842-8.

20. Navaza, J. (1994) *Acta Cryst. A50*, 157-63.

21. Sack, J. S. (1988) *J. Mol. Graphics 6*, 224-225.

22. Brunger, A. T. (1992) *X-PLOR: A System for X-Ray Crystallography and NMR*, Yale Univ. Press, New Haven.

23. Raves, M. L., Harel, M., Pang, Y. P., Silman, I., Kozikowski, A. P., & Sussman, J. L. (1997) *Nat. Struct. Biol. 4*, 57-63.

24. Kleywegt, G. J., & Brunger, A. T. (1996) *Structure 4*, 897-904.

25. Ferrin, T. E., Huang, C. C., Jarvis, L. E., & Langridge, R. (1988) *J. Mol. Graphics 6*, 13-27.

26. Laskowski, R. A., Moss, D. S., & Thornton, J. M. (1993) *J. Mol. Biol. 231*, 1049-67.

27. Hol, W. G. J., van Duijnen, P. T., & Berendsen, H. J. C. (1978) *Nature 273*, 443-446.

28. Ghosh, D., Wawrzak, Z., Pletnev, V. Z., Li, N., Kaiser, R., Pangborn, W., Jornvall, H., Erman, M., & Duax, W. L. (1995) *Structure 3*, 279-88.

29. Baba, T., Downs, D., Jackson, K. W., Tang, J., & Wang, C. S. (1991) *Biochemistry 30*, 500-10.

30. Morlock-Fitzpatrick, K. R., & Fisher, E. A. (1995) *Proc. Soc. Exp. Biol. Med. 208*, 186-190.

31. Abouakil, N., Mas, E., Bruneau, N., Benajiba, A., & Lombardo, D. (1993) *J. Biol. Chem. 268*, 25755-25763.

32. Loomes, K. M., & Senior, H. E. J. (1997) *FEBS Lett. 405*, 369-372.

33. DiPersio, L. P., Carter, C. P., & Hui, D. Y. (1994) *Biochemistry 33*, 3442-3448.

34. Brzozowski, A. M., Derewenda, U., Derewenda, Z. S., Dodson, G. G., Lawson, D. M., Turkenburg, J. P., Bjorkling, F., Huge-Jensen, B., Patkar, S. A., & Thim, L. (1991) *Nature 351*, 491-4.

35. Grochulski, P., Li, Y., Schrag, J. D., Bouthillier, F., Smith, P., Harrison, D., Rubin, B., & Cygler, M. (1993) *J. Biol. Chem. 268*, 12843-7.

36. van Tilbeurgh, H., Sarda, L., Verger, R., & Cambillau, C. (1992) *Nature 359*, 159-62.

37. Rubin, B. (1994) *Nat Struct Biol 1*, 568-72.

38. Grochulski, P., Li, Y., Schrag, J. D., & Cygler, M. (1994) *Protein Sci. 3*, 82-91.

39. Eisenhaber, F., Lijnzaad, P., Argos, P., Sander, C., & Scharf, M. (1995) *J. Comp. Chem. 16*, 273-284.

40. Kraulis, P. J. (1991) *J. Appl. Crystallogr. 24*, 946-50.

41. Merritt, E. A., & Murphy, M. E. P. (1994) *Acta Cryst. D50*, 869-73.

42. Jones, T. A., Zou, J. Y., Cowan, S. W., & Kjeldgaard, M. (1991) *Acta Crystallogr. A 47*, 110-9.

Table 1. Crystallographic data

Data collection statistics

Space group	*C*2
Unit cell (Å)	a=100.42, b=54.25, c=106.34, β=104.12
Resolution limit (Å)	1.6
Observations (all)	66076
Completeness (%) (last shell)	89.1 (68.1)
Redundancy	2.3
R_{sym} (%)	8.7
$\langle I/\sigma I \rangle$	11.5

Refinement and model statistics

Resolution (Å)	40.0-1.6
σ cutoff	2.0
Reflections	41187
R_{cryst} (%)	21.1
R_{free} (%)	25.0
Amino acids	532 (1-112, 120-533, 574-579)
Non-hydrogen atoms	4324
Water molecules	199
Average *B*-factor (Å^2)	14.044

R.m.s. Δ bond lengths (Å)	0.007
R.m.s. Δ bond angles (degrees)	1.377
Ramachandran geometry	89.4 % most favored regions
	10.2 % allowed regions
	0.2 % generously allowed regions
	0.2 % disallowed regions

Table 2. Solvent accessibility of residues upon removal of C-terminal residues 574-579[a]

Residue	Accessibility (Å^2)	Accessibility after removal of peptide (Å^2)	Exposed area (Å^2)
Q66	9.2	18.3	9.1
Y105	3.1	44.6	41.5
G106	8.2	15.6	7.4
G107	***0.3***	***27.3***	***27.0***
A108	***2.9***	***14.6***	***11.7***
F109	1.4	31.0	29.6
L110	14.3	30.5	16.2
M111	28.6	76.1	47.5
G112	85.4	120.6	35.2
A120	119.4	119.7	0.3
Y123	70.1	84.9	14.8
L124	9.8	30.7	20.9
Y125	8.4	10.6	2.2
Y143	5.2	7.4	2.2
V145	6.8	9.7	2.9
F150	2.0	15.3	13.3
E193	0.1	2.1	2.0
S194	**4.8**	**23.4**	**18.6**
A195	***2.0***	***38.6***	***36.6***

A198	0	4.2	4.2
S199	0	4.5	4.5
L202	1.0	1.4	0.4
W227	22.0	32.6	10.6
A228	0	1.2	1.2
Y270	6.5	10.3	3.8
L272	7.4	10.8	3.4
L282	17.2	17.3	0.1
L285	5.3	36.8	31.5
F287	8.7	15.5	6.8
V288	3.8	21.3	17.5
P289	0	12.9	12.9
L323	27.9	37.2	9.3
F324	3.9	21.2	17.3
M327	44.2	47.6	3.4
H435	**3.8**	**15.5**	**11.7**
A436	4.8	29.3	24.5
L439	5.6	7.4	1.8

[a]Catalytic residues are indicated in bold, and the putative oxyanion binding residues are in bold italics. Calculation of solvent accessible area done using ASC (39).

Table 3. Alignment of C-terminal residues of mammalian CEases

Rat	VEAQMPVAIGF
Bovine	EVAQMPVVIGF
Rabbit	VAAQMPMAIGF
Human	KEAQMPAVIRF
Mouse	VEAQMPATIGF

FIGURE LEGENDS

Figure 1: Electrophoretic characterization of mutant and native CEases. (a) SDS-PAGE, (b) IEF gel, (c) native PAGE. Molecular weight and IEF standards are indicated by S, and mutant and native CEases are indicated by M and N, respectively.

Figure 2: Functional analysis of mutant and native CEase. (a) Cholesteryl [1-^{14}C] oleate hydrolysis vs. added enzyme. (b) Cholesteryl [1-^{14}C] oleate hydrolysis vs. pH. (c) Cholesteryl [1-^{14}C] oleate hydrolysis vs. TC. (d) p-NPB hydrolysis vs. TC and pH. CEase concentration was at 25 ng/275 µl for cholesteryl [1-^{14}C] oleate hydrolysis experiments, in the presence of 4 mM TC. p-NPB hydrolysis experiments were performed at 0.02 mg/ml CEase. Squares and diamonds represent native and mutant CEase, respectively, and buffer blanks are indicated as circles.

Figure 3: Topology and structure of bovine pancreatic CEase. The catalytic triad of Asp 320, His 435, and Ser 194 is shown in ball-and-stick representation at the center, and the putative heparin binding domain is shown at the lower right, consisting of residues 56-63. This figure was generated using MOLSCRIPT (40).

Figure 4: Representative N-terminal electron density. A $2F_o$-F_c map was calculated to 1.6 Å resolution and contoured at 1 σ. The map shows clear electron density in an N-terminus beta sheet region of CEase. This figure was generated using MOLSCRIPT (40).

Figure 5: Structure of the active site region of CEase. Active site residues Ser 194, Asp 320, and His 435 are labeled. Putative oxyanion coordinating residues Ala 195, Gly 107, and Ala 108 are highlighted in italics, and C-terminal residues 574-579 are labeled. Water molecules close to Ser 194 are indicated as spheres. This figure was generated using MOLSCRIPT (40) and Raster3D (41).

Figure 6: (a) Alpha carbon alignment of the residues in the active site region of CEase (black) and *Torpedo californica* acetylcholinesterase (gray). Residues in lowercase correspond to acetylcholinesterase, and residues in uppercase correspond to pancreatic CEase. Conserved Tyr 105 in CEase is flipped with respect to Tyr 116 in acetylcholinesterase, and the C-terminus of CEase diverts the oxyanion binding loop away from catalytic Ser 194 in the apoenzyme structure. The orientation of the oxyanion loop in acetylcholinesterase may represent the structure of CEase in this region in the activated state of the enzyme. (b) Alpha carbon alignment of the N-terminus of CEase and *Candida cylindracea* CEase. Amino acids 61-210 of CEase (black) were aligned with the corresponding residues of *Candida cylindracea* CEase (gray). Comparison of the regions enclosed by the N-terminal disulfide loop regions shows a truncated loop in CEase, and a helical lid in *Candida cylindracea* CEase. The disulfide bridge (Cys 64-Cys80) is indicated, and the active site Ser 194 is shown in ball-and-stick representation. This figure was generated using MOLSCRIPT (40), Raster3D (41), and O (42).

Figure 7: Electrostatic potential and temperature factor profiles of CEase. (a) Potential diagram ramped from -10/kT (red) to +10/kT (blue). The putative heparin binding site lies at the area of positive potential at the lower left, with Arg 63 indicated. (b) Temperature factor diagram of active site face of bovine pancreatic CEase. The catalytic His 435 is indicated, with temperature factors ramped from blue (low temperature factors) to red (high temperature factors). The areas of high temperature factors and negative potential are coincident, notably in the helical region of amino acids 322-376 at the upper right. Figure generated using GRASP (43).

Figure 8: Stereodiagram of proposed Michaelis complex between CEase (black) and cholesteryl linoleate (gray). Active site residues are indicated, and putative oxyanion coordinating residues Ala 195, Gly 107, and Ala 108 are in lowercase. The cholesteryl linoleate molecule spatially overlaps with C-terminal residues 574-579. Docking was done using MIDAS (25). This figure was generated using MOLSCRIPT(40) and Raster3D (41).

Figure 9: Active site hydrogen bond network and proposed mechanism and stereochemistry of the tetrahedral intermediate in the ester hydrolysis reaction. The NH of Ala 195 is in a position to coordinate the oxyanion, and the loop containing Gly 107 may move into a productive binding position to act as a second hydrogen bond donor to the oxyanion.

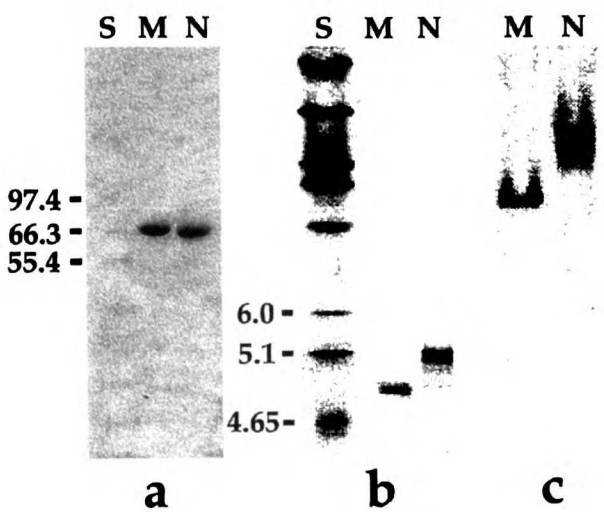

Figure 1.

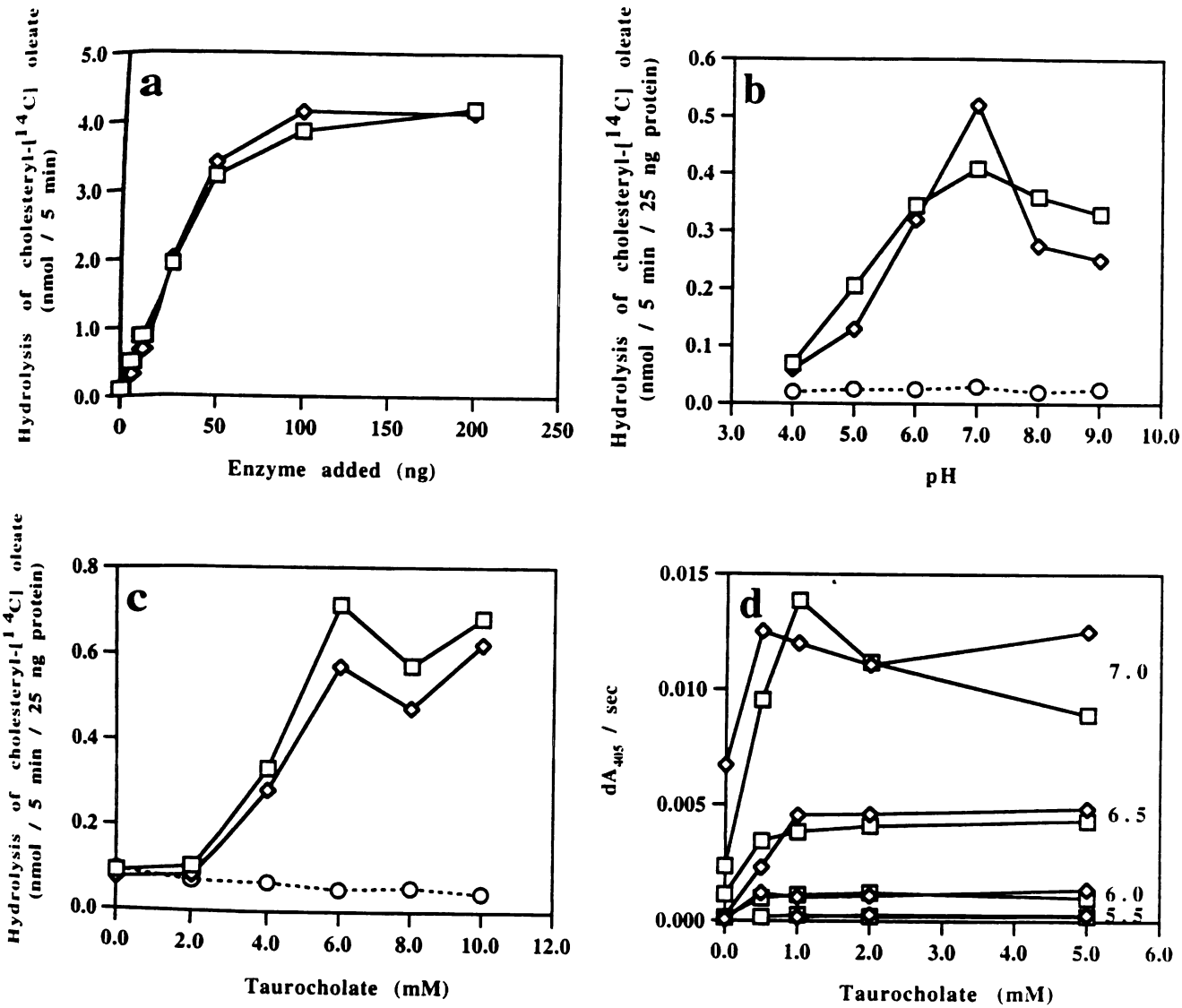
a
Hydrolysis of cholesteryl-[14C] oleate (nmol / 5 min)
Enzyme added (ng)
b
Hydrolysis of cholesteryl-[14C] oleate (nmol / 5 min / 25 ng protein)
pH
c
Hydrolysis of cholesteryl-[14C] oleate (nmol / 5 min / 25 ng protein)
Taurocholate (mM)
d
dA405 / sec
7.0
6.5
6.0
5.5
Taurocholate (mM)

Figure 2.

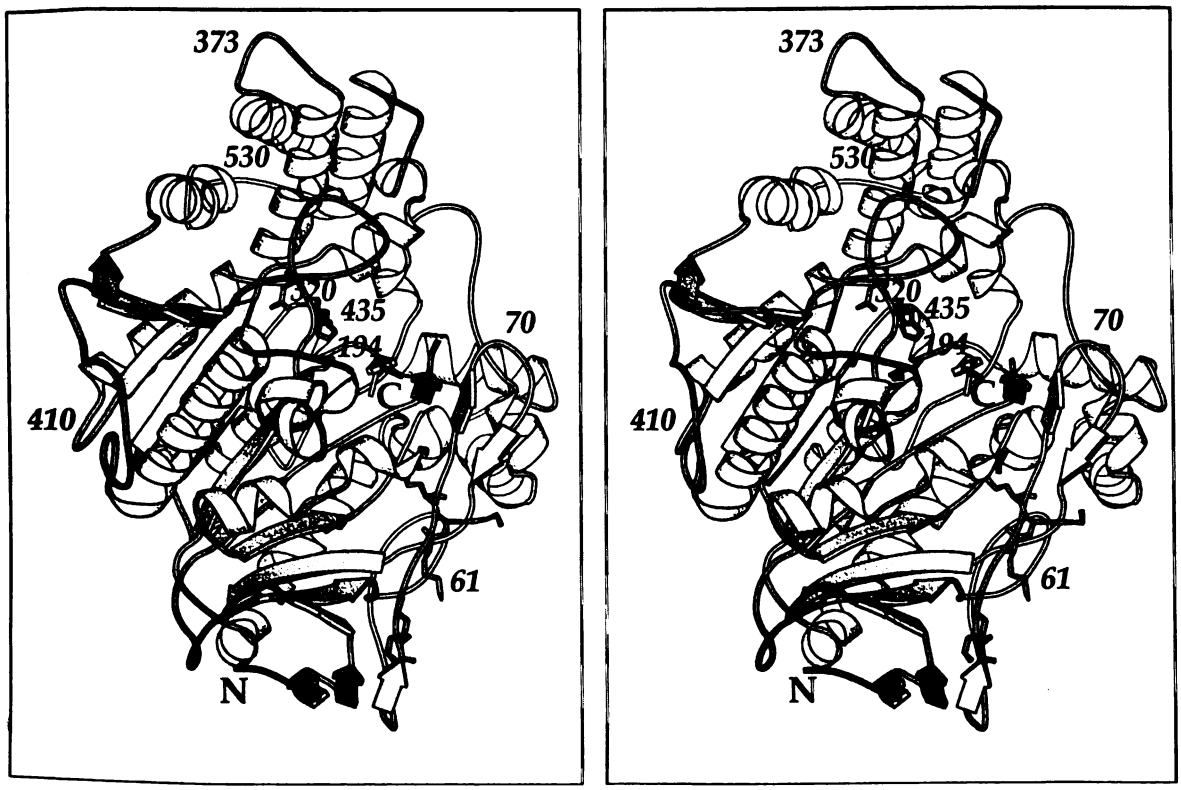

Figure 3.

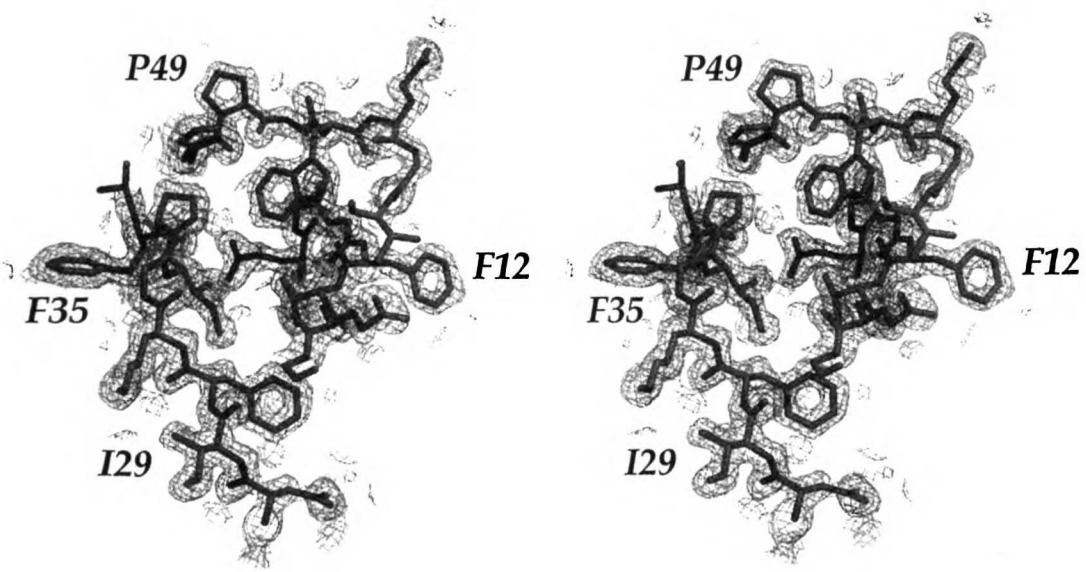

Figure 4.

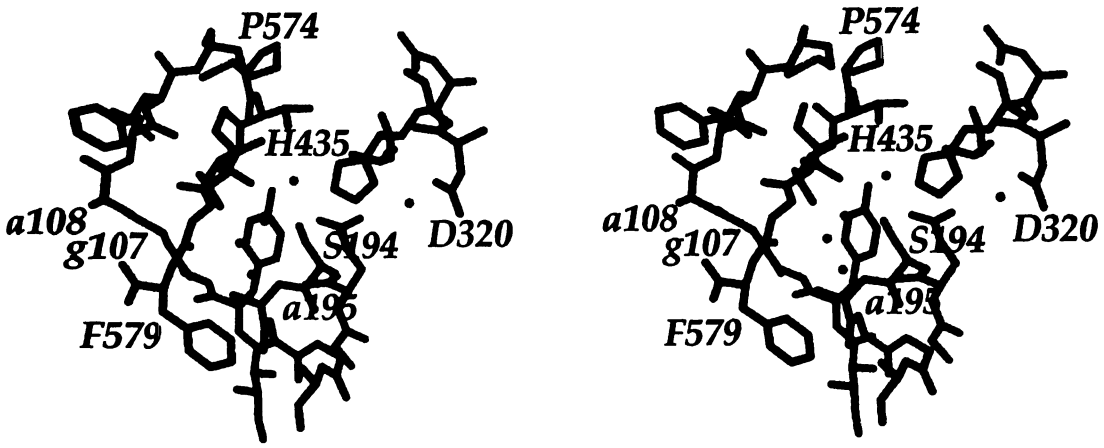
P574
H435
a108
g107
S194
D320
a195
F579
P574
H435
a108
g107
S194
D320
a195
F579

Figure 5.

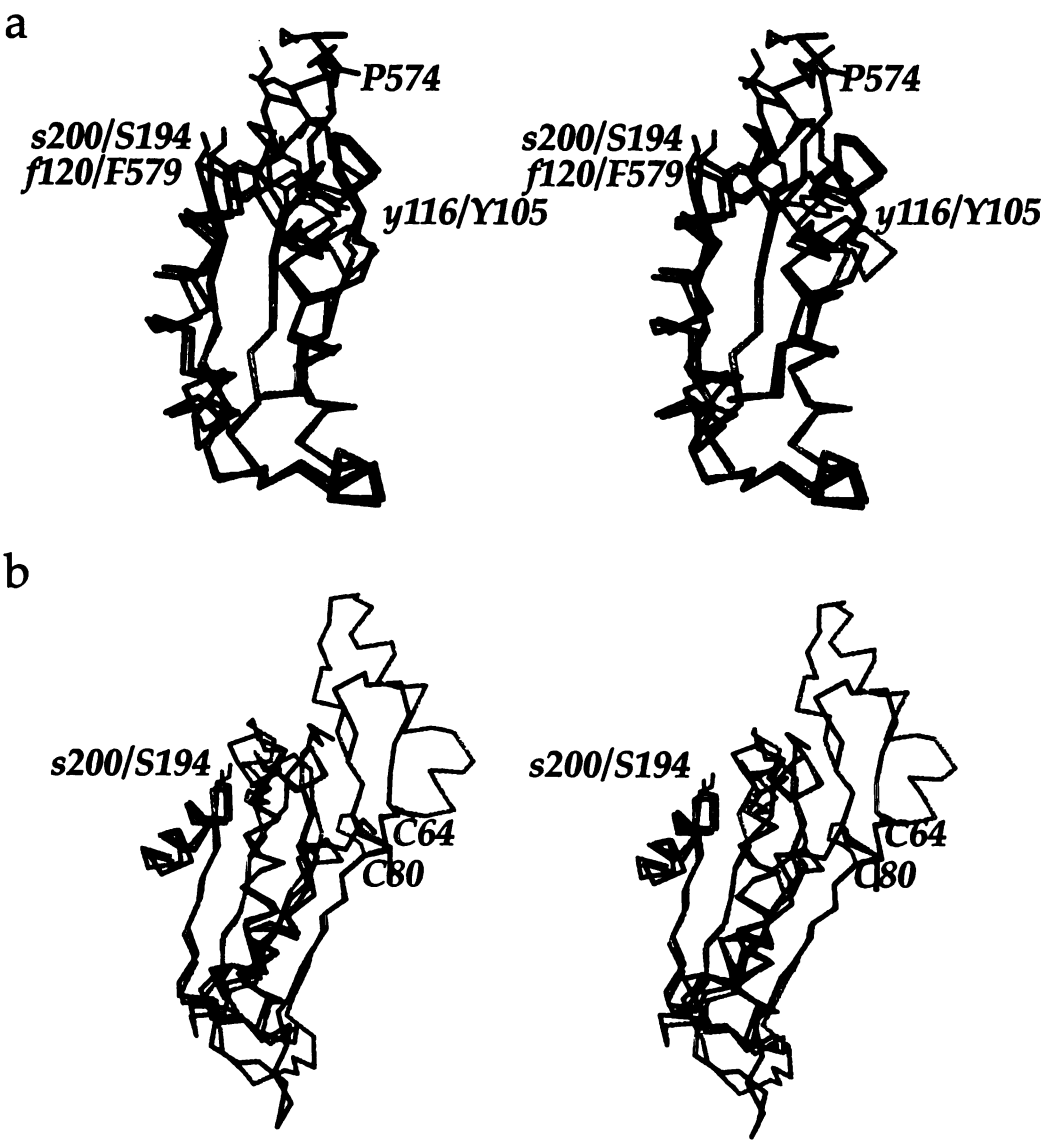
a
P574
s200/S194
f120/F579
y116/Y105
P574
s200/S194
f120/F579
y116/Y105
b
s200/S194
C64
C80
s200/S194
C64
C80

Figure 6.

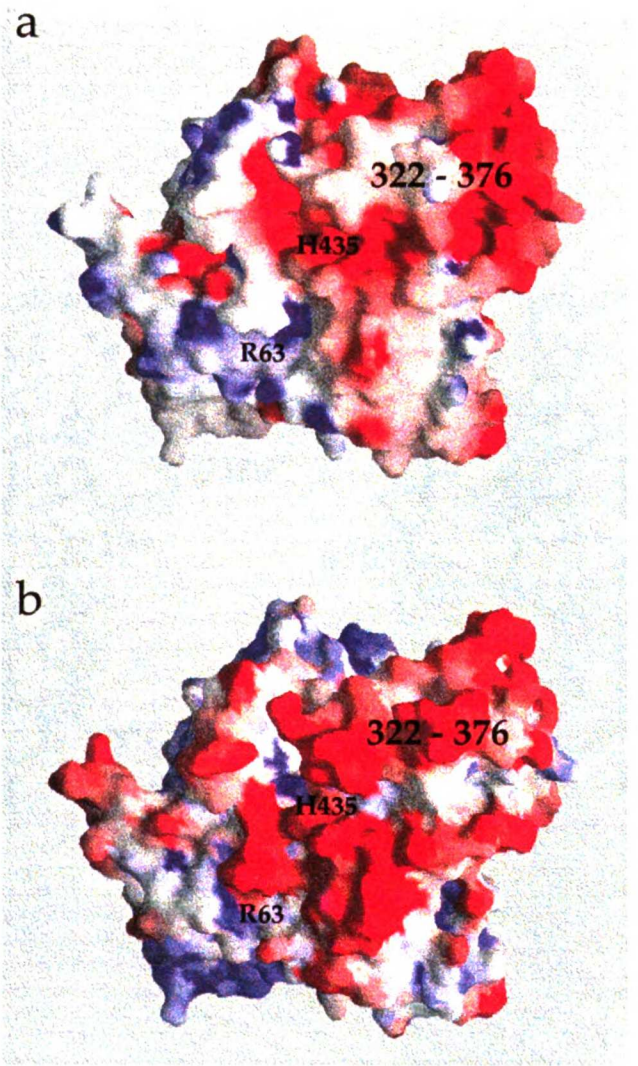

Figure 7.

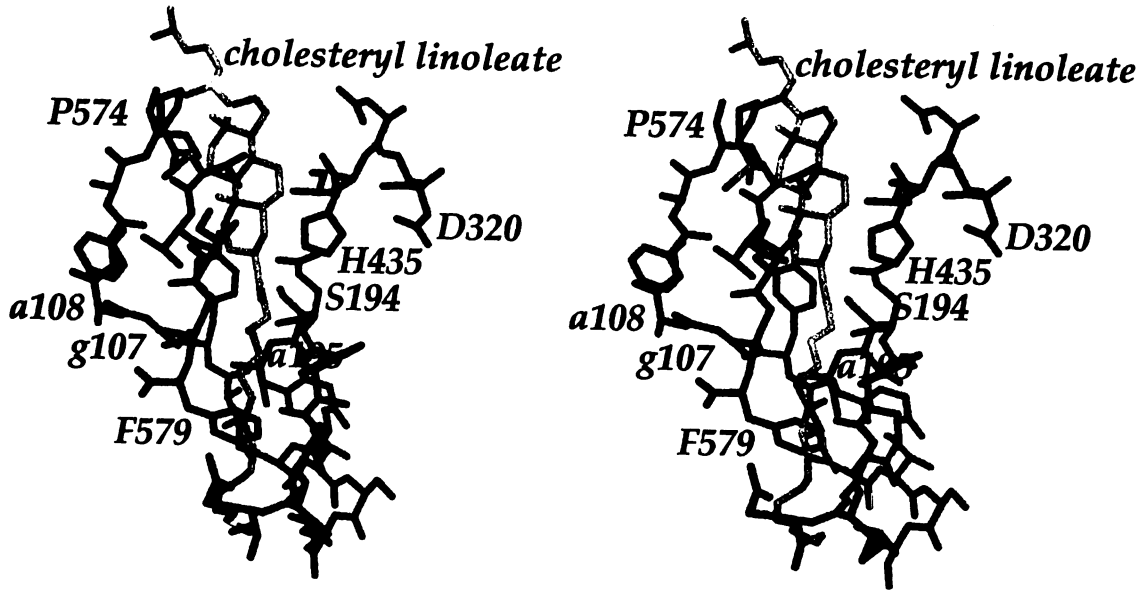
cholesteryl linoleate
P574
D320
H435
S194
a108
g107
F579
cholesteryl linoleate
P574
D320
H435
S194
a108
g107
F579

Figure 8.

Figure 9.

Chapter 2

The structure of a new crystal form of bile-salt activated lipase highlights biologically relevant domain motions

The structure of a new crystal form of bile-salt activated lipase highlights biologically relevant domain motions

Julian C.-H. Chen, Larry J.W. Miercke, Jolanta Krucinski, and Robert M. Stroud

Graduate Group in Biophysics and Department of Biochemistry and Biophysics, Box 0448, University of California, San Francisco, CA 94143

Running title: Multiple conformations of cholesterol esterase

Coordinates have been deposited in the PDB with code xxxx.

ABBREVIATIONS AND TEXTUAL FOOTNOTES

MES, 2-(*N*-morpholino)ethanesulfonic acid

CMC, critical micelle concentration

DLS, dynamic light scattering

PEG, polyethylene glycol

BSA, bovine serum albumin

RMSD, root mean square deviation

NCS, non-crystallographic symmetry

CNS, Crystallography and NMR System

ABSTRACT

A new crystal form of the unliganded form of the bile salt activated lipase cholesterol esterase from bovine pancreas has been obtained and solved to 2.0 Å resolution (space group $P2_12_12$, a=141.353 Å, b=178.662 Å, c=95.31 Å, $\alpha=\beta=\gamma=90$, R_{free} = 24.4 %, R_{cryst}=21.5 %). Strikingly, the three monomers in the asymmetric unit are in significantly different conformations, with root mean squared deviations (rmsd) of 0.48-0.87 Å between them overall. A comparison with the two other cholesterol esterase apoenzyme structures in the PDB reveals up to 1.25 Å rmsd between these five structures. Superpositions of these five structures highlight domain movements and infer dynamics in cholesterol esterase. A concerted domain shift involving the 422-436 loop coupled to the 318-390 helical bundle region moves the catalytic His435 in and out of hydrogen bonding position with respect to other members of the catalytic triad, which remain relatively fixed in conformation. This area lies in the cleft that binds a bile salt molecule in the taurocholate-bound structure of cholesterol esterase. The bile salt loop (residues 105-126) adopts multiple conformations, rendering the active site serine and histidine inaccessible to substrate. We propose that this conformational variability throughout the protein and the ability of the bile salt loop to adopt alternative, stable structures explain the low basal activity of the enzyme. The addition of bile salt may stabilize the catalytic triad in a productive conformation in addition to permitting access of the substrate to the active site. The conformational flexibility of this lipase may also allow for its wide substrate specificity.

Cholesterol esterase, also known as bile salt activated lipase, is a primary lipase in the digestion of dietary triglycerides and phospholipids, in addition to being the sole enzyme responsible for hydrolyzing cholesterol esters and vitamin esters (1). Cholesterol esterase is dependent on bile salts such as taurocholate for optimal activity, in contrast to other lipases which act interfacially, at an oil-water interface (2). Its low basal activity against substrates is enhanced by addition of submicellar concentrations of activating bile salts with an apparent K_d of ~400 μM, far below its critical micelle concentration (CMC) of ~5 mM (3).

However, it is not clear structurally how cholesterol esterase is activated by bile salts. Two crystal structures of the apoenzyme form and one structure of the bile salt taurocholate bound form have been solved at 2.8 Å, 1.6 Å, and 2.8 Å resolution, respectively (4, 5). The two apoenzyme structures are significantly different from one another, in the conformation of the bile salt binding loop and notably in the presence of the C-terminus lodged in the active site in our earlier, 1.6 Å apoenzyme structure (4). Our earlier structure shows putative oxyanion stabilizing residues in the bile salt loop displaced by the C-terminus and a putative fatty acid binding pocket occupied by the hydrophobic last six residues of the enzyme. Due to these differences in the apoenzyme structures, the conformational transitions that take place upon binding bile salt remain unclear.

The 2.8 Å structure of cholesterol esterase complexed with the activating bile salt taurocholate shows two molecules of bile salt bound per monomer of enzyme (5). The role of the binding site proximal to the catalytic triad is clear, exposing a surface for substrate binding and catalysis by ordering the bile salt loop away from the active site. However, the function of the distal site, located in a shallow cleft away from the active site, is not known, although biochemical

studies have demonstrated the presence of more than one bile salt binding site on cholesterol esterase (6, 7). Therefore, in contrast to classical triglyceride lipases, which are activated by the opening of a 'lid' region at an oil-water interface to expose the active site catalytic triad to substrate, activation of cholesterol esterase by bile salts is a more complex process, possibly involving subtle structural rearrangements in addition to ordering the bile salt loop (2). In order to better understand the conformational transition between the apoenzyme and bile salt bound, activated enzyme, we have obtained crystals of bovine pancreatic cholesterol esterase grown in the presence of bile salts and in their absence. The structure of the new apoenzyme crystal form presented here contains multiple copies of the enzyme in the asymmetric unit and highlights domain motions as important in the function of cholesterol esterase.

MATERIALS AND METHODS

Purification. Native wild-type cholesterol esterase from bovine pancreas was purified on S-sepharose and SP-sephadex columns using a previously described protocol, with one additional step (8). The pooled fraction from SP-sephadex was concentrated, and dialyzed overnight against 20 mM MES pH 6.0, 50 mM NaCl. The dialyzed target was filtered and injected into a 1.2 cm x 10 cm Poros HS strong cation exchanger (Perseptive Biosystems) run at 4 ml/min in 20 mM MES pH 6.0. A 5 minute 0 M to 0.45 M NaCl gradient was run 1 minute post injection, with the target enzyme eluting at ~0.12 M NaCl.

Molecular size characterization. Hydrodynamic stoichiometry and molecular weight were assessed using a DynoPro-801 Dynamic Light Scattering/Molecular Sizing Instrument equipped with a micro-cuvette based MicroSampler (Protein Solutions). Measurements were performed on a sample concentrated to 2 mg/ml buffered with Na-acetate 5.0 and 50 mM NaCl. The stoichiometry of the apoenzyme in solution is confirmed by dynamic light scattering, which shows a narrow monomodal size distribution of the 64 kDa monomeric species as judged by a baseline of 1.000 and polydispersity of 5%.

Crystallization. Purified native bovine pancreatic cholesterol esterase was concentrated to approximately 5 ml, dialyzed 48 hours against 2 L 25 mM Na-acetate pH 5.1 and 100 mM NaCl. The protein was further concentrated to 5-6 mg/ml for crystallization trials. All protein samples were concentrated by high-pressure stirred cell ultrafiltration using YM-10 membranes (Amicon) and filtered using 0.8/0.2 μm syringe filters from Gelman (part #4187). Protein concentration was determined by the Bradford assay using bovine serum albumin (BSA) as a standard.

Preliminary crystals were obtained in a polyethylene glycol (PEG) condition using factorial screening kits (Hampton Research). They appeared in about 4-5 days and often grew as tiny plates and thin rods. Subsequently conditions were optimized using a fine screen between 16 to 24 % PEG 3000. The pH of these conditions varied from 5.9 to 6.5, and addition of salts such as 0.2 M ammonium sulfate and Na-phosphate appeared to enhance crystallization and facilitate crystal growth.

Data collection. Data were collected at Stanford Synchrotron Radiation Laboratory Beamline 7-1 (λ=1.08 Å) on a 30 cm image plate (MAR Research). The

crystal was transferred quickly from the drop to a 7 µl solution of cryosolvent composed of 25 % PEG 3000, 80 mM Na-citrate pH 6.5, 50 mM NaCl and 0.2 M ammonium sulfate or Na-phosphate solution containing 20 % glycerol as a cryoprotectant. The crystal was then flash frozen in a nitrogen gas stream at 90 K. Data were indexed, integrated, and scaled using DENZO/SCALEPACK (9) with no σ cutoff, indexing in space group $P2_12_12$ with cell dimensions a=141.353 Å, b=178.662 Å, c=95.31 Å, $\alpha=\beta=\gamma=90$. Prior to refinement, a 5 % set of reflections between 500 and 2.0 Å resolution were set aside for calculating R_{free} (10, 11).

Structure solution and analysis. A refined model of the taurocholate bound complex independently solved by our group, which crystallized in the same space group and had very similar cell dimensions (following chapter), was used as an initial model for generating difference maps, with the ligand, water molecules, and glycosylation removed from the model. The initial model had a starting R-factor of 31.9 %, and this was subjected to a refinement cycle of conjugate gradient, individual temperature factor, and torsional simulated annealing minimization in CNS (Crystallography and NMR System) to remove model bias (12-15). The resulting $2F_o$-F_c and F_o-F_c maps revealed additional features in the electron density, which were manually built in using CHAIN (16). Several additional rounds of model building followed by refinement in CNS reduced the R_{free} to 24.40 % and the R_{cryst} to 21.54 %. Due to significant structural differences among the three monomers in the asymmetric unit, non-crystallographic symmetry (NCS) restraints were not used in the course of the refinement. The fit of the model was confirmed by calculating a composite

simulated annealing omit map in CNS. The quality of the structure is summarized in Table 1.

Comparisons and overlays of the three-dimensional structures of cholesterol esterase were done using the O utility LSQMAN with a 3.8 Å cutoff for calculation of root mean squared deviations (17). PROCHECK was used to monitor Ramachandran parameters (18). Figures were generated using MOLSCRIPT (19) and Raster 3D (20).

RESULTS

Crystal structure. The asymmetric unit of this crystal form of the cholesterol esterase apoenzyme contains three molecules (A, B, and C) packed in unique environments not related by any simple non-crystallographic symmetry operations or any complementary interactions (Figure 1). The overall architecture of the three monomers in the asymmetric unit is similar, with a mixed α and β structure belonging to the α-β hydrolase superfamily. Triglyceride lipases and other esterases share this same basic fold. The C terminal proline-rich repeat domain (residues 540-573) is disordered in each of the monomers, consistent with the structures solved previously.

Monomers A and B are essentially structurally identical, sharing similar bile salt loop conformations and an overall Cα rmsd of 0.479 Å. Monomer C is unique, having an extended bile salt loop structure and rmsds of 0.869 Å and 0.895 Å from Monomer A and B, respectively (Table 2). This is greater than the estimated Luzzati coordinate error of 0.27 Å (21). Monomer C contains extensive

crystal contacts, mainly with Monomer B and to a lesser extent with Monomer A. Contacts between Monomers A and B are much more limited. The active sites of Monomers A and B face each other, but do not suggest a physiological interaction, due to minimal contacts between the two monomers and a lack of significant buried surface area.

Surprisingly, the hydrophobic extreme C terminus composed of amino acids 574-579 found in our earlier apoenzyme structure is missing in all three monomers solved here (4). In our earlier structure, the C terminus is lodged in a putative fatty acid binding pocket, displacing the oxyanion hole away from a productive binding position. The differences in these structures may be explained in part by the crystallization conditions used in our earlier, 1.6 Å apoenzyme structure. The less polar PEG condition used to crystallize the orthorhombic form of cholesterol esterase may allow more favorable interactions between the hydrophobic C terminus and the PEG. However, in the context of the physiological environment of the enzyme, a mixed hydrophilic/hydrophobic environment, the C terminus is in a biologically relevant conformation when lodged in the active site.

A comparison of the five apoenzyme structures of bovine pancreatic cholesterol esterase (PDB code 1akn, 2bce, Monomer A, Monomer B, and Monomer C) shows significant differences from one another (5). In contrast with other lipases studied in multiple crystal forms, which show minimal differences between the structures, these five structures of cholesterol esterase have an average 0.864 Å rmsd from one another, ranging from 0.479 Å to 1.251 Å (Table 2). This suggests an inherent flexibility in the molecule that may be important in bile salt activation of cholesterol esterase and/or substrate binding.

Catalytic triad. The conformations of the catalytic triads of the three monomers in our crystal form show variability. Monomers A and B have similar catalytic triad conformations, with good hydrogen bonding geometry and distances between the Ser194, His435, and Asp320 (Figure 2). In contrast, in Monomer C, the εN of His435 is hydrogen bonded to a water molecule, and the Ser194 hydroxyl is no longer in good hydrogen bonding geometry and distance (3.36 Å) from the εN of His435. A comparison of the active site catalytic triads from the three monomers in the orthorhombic crystal form with the our previous apoenzyme structure and the structure solved by Wang, et al. shows a clear trend upon alignment (Table 3). The Ser194 γO – Asp320 carboxyl oxygen distance remains relatively fixed, ranging from 7.30 Å (Monomers A and C) to 7.46 Å (2bce). However, the position of the His435 relative to the other members of the catalytic triad is variable. The Ser194 hydroxyl – His435 εN distance ranges from 2.75 Å (2bce) to 3.36 Å (Monomer C). The Asp320 carboxyl – His435 δN2 distance ranges from 2.70 Å (Monomer A) to 3.08 Å (2bce). This variability in the position of His435 may be mechanistically important.

Bile salt loop conformations. The most significant differences in the three monomers lie in the conformation and secondary structure of the bile salt loop (residues Tyr105-Asp126) (Figure 4). Monomers A and B have similar bile salt loop conformations, with an alpha-helix followed by an extended loop, with elevated temperature factors in this region compared to other parts of the molecules. In contrast, Monomer C has a very well defined, rigid bile salt loop, with an extended structure that is diverted approximately 90 degrees away from the conformation in Monomers A and B. Temperature factors in this region of

Monomer C are comparable to the core region of the protein with very clear electron density, indicative of a rigid loop conformation. A further comparison with the two apoenzyme structures available in the PDB shows still different bile salt loop conformations, with poorly ordered loop conformations with no regular secondary structures (4, 5). The accessible surface area of catalytic residues Ser194 and His435 is minimal regardless of the conformation of the loop, however, it is plausible that motions and flexibility in the loop may render it partially accessible to substrates.

DISCUSSION

Comparison with other triglyceride lipases. This crystal form of cholesterol esterase provides a rare opportunity to observe the enzyme in an ensemble of structures corresponding to low-energy conformations, the crystallographic equivalent of an NMR structure. Compared to other triglyceride lipases, cholesterol esterase shows a more complicated set of motions.

A comparison of the open and closed structures of the lipase from *Candida rugosa* at 2.0 Å resolution show very little overall conformational change, with a 0.3 Å rmsd between the two states, excluding the lid region (22-24). Crystals of the open and closed forms grow in different space groups and under entirely different conditions. These structures therefore suggest that the dynamics of the protein are limited exclusively to the lid region. A structure of *Pseudomonas cepacia* lipase at 2.1 Å resolution shows two monomers in the asymmetric unit differing by a rmsd of 0.14 Å for mainchain atoms (25). A structure of the same

lipase solved in three different laboratories at 2.0-2.2 Å resolution differs by a rmsd of 0.3 Å over mainchain atoms, again suggesting dynamics localized to the lid region (26). The structure of two crystal forms of the lipase B from *Candida antarctica* at 1.55 Å and 2.1 Å resolution reveals a 0.24 Å rmsd over the Cα atoms (27). In these three cases, the differences in the structures are comparable to the estimated Luzzati coordinate errors (21). Therefore, the significant rmsd values found between the five apoeznyme structures of cholesterol esterase are most likely indicative of true conformational variability relating to the biological function of the enzyme (Table 2).

Domain motions in cholesterol esterase. A least squares superposition of the five apoenzyme structures of cholesterol esterase (Figure 3) identifies several major areas that show significant variation. The bile salt loop (residues 105-126) shows the greatest variety of conformations. This loop assumes numerous structures, from a helical structure in Monomers A and B to an ordered, extended structure in Monomer C, and disordered loops with poor electron density and high temperature factors in the structures of Wang, et al. and Chen, et al.

The most significant variation, however, is in the helical bundle region following catalytic Asp320. The backbone diverges in the five structures, and appears to be coupled to the position of catalytic His435, causing a shift of up to 0.61 Å in the position of the histidine. In the five apoenzyme structures, a conserved set of hydrogen bonds between the 422-436 loop and the 318-390 region allows the helical region and the loop to move as a unit. The side chains of His322 and Asp434 interact with each other, and the side chain of Asp318 interacts with the main chain amide of Ala433. This coupled domain

rearrangement is sufficient to position the histidine in and out of good hydrogen bonding geometry and distance for catalysis. While this region in Monomer C is involved in a number of crystal contacts with Monomer B, the rearrangement that shifts the active site conformation involves a concerted movement of the 422-436 loop and the 318-390 region. The involvement of more than 80 residues makes it unlikely that crystal packing forces can account for this degree of movement, and we therefore consider this movement to be inherent to the protein.

In addition to these two important movements in the bile salt loop and the region containing residues 422-236 and 318-390, the loop contained within disulfide bridged residues 64 and 80 is variable. A stretch between residues 270 and 287 is also flexible, and consequently has the poorest electron density of any part of the molecule. Nevertheless this loop assumes a similar orientation in the five monomers, though displaced by several Å rmsd.

Biological implications. Cholesterol esterase has a low basal activity in the absence of activating bile salts. Based on the five structures of the apoenzyme now available, the low basal activity is only partially explained by the bile salt loop blocking the active site, as multiple conformations for the loop are observed, with varying degrees of accessibility to the active site. More importantly, the enzyme may be in an equilibrium of conformational states, of which only a subset are competent for catalysis. Monomer C exhibits one such case of an inactive conformational state. While it may be argued that the active site is not fully formed until substrate is bound, four out of the five structures of the apoenzyme show a preformed catalytic triad, therefore most likely Monomer C is a true apoenzyme conformation.

A role for bile salt binding. In the 2.8 Å taurocholate-bound structure of cholesterol esterase, two bile salt binding sites were found, with one molecule directly involved in ordering the proximal bile salt loop (Tyr105-Asp126), and the second, distal molecule bound in a cleft > 10 Å from the catalytic serine (5). The taurocholate molecule that interacts with the bile salt loop diverts the loop away from the active site, rendering catalytic triad accessible to large hydrophobic substrates such as cholesterol esters and triglycerides. This distal cleft may be a high-affinity site that stabilizes a competent active site conformation. Strikingly, the area of domain movement responsible for shifting the catalytic histidine into hydrogen bonding position is coincident with the cleft that binds the distal bile salt molecule. It is therefore possible that bile salt binding may order this domain, and hence shift the equilibrium towards an active site competent conformation. This is a prerequisite for enzymatic activity, therefore it makes sense that the distal bile salt binding site is of higher affinity than the site responsible for ordering the bile salt loop. Biochemical studies have presented evidence of two sites for bile salt binding (6, 7). The distal site may be a high-affinity site that is saturated at concentrations well below the apparent K_d found in the enzymatic activity-coupled assays for bile salt dependence (400 μM) such that the distal site is not detected. Binding assays sensitive to molecular weight changes, such as surface plasmon resonance, could be used to test this hypothesis.

The fact that cholesterol esterase has a low basal activity in the absence of bile salts may be explained by two factors: the disorder of the bile salt loop prevents effective substrate access to the active site, and variation in the

geometry of the apoenzyme catalytic triad conformations further decreases the apparent activity.

Another explanation for the wide variety of apoenzyme conformations is that the flexibility is inherent and allows for the wide substrate specificity of the enzyme. Cholesterol esterase is responsible for hydrolyzing a wide variety of substrates, from cholesterol esters to phospholipids and triglycerides, and the flexibility of the enzyme may allow for this promiscuity.

Whether the activated enzyme shows such conformational flexibility is not well-established. While the 2.8 Å structure of cholesterol esterase complexed with taurocholate shows minimal differences between the two molecules in the asymmetric unit (~0.23 Å rmsd), this may be due to the low resolution of their structure and the subsequent use of NCS during refinement (5). A high resolution structure of the activated complex will be necessary to distinguish whether the conformational flexibility seen in the apoenzyme structures is inherent or whether binding of bile salt orders the enzyme into a more fixed conformation.

These five structures are in essence a high-resolution NMR structure, and represent equilibrium states of the molecule. Out of these, a fraction of conformations have active sites both accessible to solvent and triglycerides and a fraction of conformations have competent active site geometry. We propose a role for bile salt binding in enhancement of the activity of cholesterol esterase. First, as seen in the taurocholate/cholesterol esterase structure of Wang, et al., it orders the bile salt loop away from the catalytic triad allowing access of substrate to the active site. Second, we propose that bile salt stabilizes the catalytic triad by

binding to the distal site and bringing the histidine into a productive hydrogen bonding arrangement for catalysis.

Our structures of the apoenzyme of bovine pancreatic cholesterol esterase highlight a crucial difference between this and other triglyceride lipases. The five available structures of the bovine pancreatic cholesterol esterase apoenzyme available show a wide variety of stable, alternative conformations. This is in contrast to the triglyceride lipases, which show very little apparent dynamic behavior outside their lid regions.

Lipase activation has been extensively studied in fungal and bacterial lipases as well as pancreatic lipase. Only recently have the structures of cholesterol esterase in their apoenzyme and bile salt bound, activated forms been reported. With these new structures of the cholesterol esterase apoenzyme, it is clear that activation of the enzyme by bile salts is a complex process, and not a simple closed to open transition found in other triglyceride lipases.

ACKNOWLEDGMENTS

We thank Drs. Amy Anderson, Tim Fritz, and Janet Finer-Moore for critical discussions, and David Sullivan for providing a program for analyzing domain movements. We thank Xingbo Wang (CV Therapeutics, Inc.) for providing protein.

REFERENCES

1. Hui, D. Y. (1996) *Biochem. Biophys. Acta 1303*, 1-14.

2. Rubin, B. (1994) *Nat Struct Biol 1*, 568-72.

3. Wang, C. S., & Hartsuck, J. A. (1993) *Biochem. Biophys. Acta 1166*, 1-19.

4. Chen, J. C.-H., Miercke, L.J.W., Krucinski, J., Starr, J.R., Saenz, G., Wang, X., Spilburg, C.A., Lange, L.G., Ellsworth, J.L., and Stroud, R.M. (1998) *Biochemistry 37*, 5107-5117.

5. Wang, X., Wang, C.-S., Tang, J., Dyda, F., & Zhang, X. C. (1997) *Structure 5*, 1209-1218.

6. Blackberg, L., & Hernell, O. (1993) *FEBS Lett. 323*, 207-210.

7. Tsujita, T., Mizuno, N.K., and Brockman, H.L. (1987) *J. Lipid Res. 28*, 1434-1443.

8. Spilburg, C. A., Cox, D. G., Wang, X., Bernat, B. A., Bosner, M. S., & Lange, L. G. (1995) *Biochemistry 34*, 15532-8.

9. Otwinowski, Z. (1993) in *Data Collection and Processing* (Sawyer, L., Isaacs, N. W., & Bailey, S., Eds.) pp 556-562, SERC Daresbury Laboratory, Warrington.

10. Brunger, A. T. (1992) *Nature 355*, 472-475.

11. Kleywegt, G. J., & Brunger, A. T. (1996) *Structure 4*, 897-904.

12. Brunger, A. T., Adams, P. D., Clore, G. M., DeLano, W. L., Gros, P., Grosse-Kunstleve, R. W., Kuszewski, J., Nilges, M., Pannu, N. S., Read, R. J., Rice, L. M., Simonson, T., & Warren, G. L. (1998) *Acta Crystallogr. D Biol. Crystallogr. 54*, 905-921.

13. Brunger, A. T., Adams, P. D., & Rice, L. M. (1997) *Structure 5*, 325-36.

14. Adams, P. D., Pannu, N. S., Read, R. J., & Brunger, A. T. (1997) *Proc. Natl. Acad. Sci. 94*, 5018-5023.

15. Pannu, N. S., & Read, R. J. (1996) *Acta Crystallogr. A 52*, 659-668.

16. Sack, J. S. (1988) *J. Mol. Graphics 6*, 224-225.

17. Jones, T. A., Zou, J. Y., Cowan, S. W., & Kjeldgaard, M. (1991) *Acta Crystallogr. A 47*, 110-9.

18. Laskowski, R. A., Moss, D. S., & Thornton, J. M. (1993) *J. Mol. Biol. 231*, 1049-67.

19. Kraulis, P. J. (1991) *J. Appl. Crystallogr. 24*, 946-50.

20. Merritt, E. A., & Murphy, M. E. P. (1994) *Acta Cryst. D50*, 869-73.

21. Luzzati, V. (1952) *Acta Crystallogr. 5*, 802-810.

22. Grochulski, P., Li, Y., Schrag, J. D., Bouthillier, F., Smith, P., Harrison, D., Rubin, B., & Cygler, M. (1993) *J. Biol. Chem. 268*, 12843-7.

23. Grochulski, P., Bouthillier, F., Kazlauskas, R. J., Serreqi, A. N., Schrag, J. D., Ziomek, E., & Cygler, M. (1994) *Biochemistry 33*, 3494-500.

24. Grochulski, P., Li, Y., Schrag, J. D., & Cygler, M. (1994) *Protein Sci. 3*, 82-91.

25. Kim, K. K., Song, H.K., Shin, D.H., Hwang, K.Y., and Suh, S.W. (1997) *Structure 5*, 173-185.

26. Schrag, J. D., Li, Y., Cygler, M., Lang, D., Burgdorf, T., Hecht, H. J., Schmid, R., Schomburg, D., Rydel, T. J., Oliver, J. D., Strickland, L. C., Dunaway, C. M., Larson, S. B., Day, J., & McPherson, A. (1997) *Structure 5*, 187-202.

27. Uppenberg, J., Hansen, M. T., Patkar, S., & Jones, T. A. (1994) *Structure 2*, 293-308.

Table 1. Crystallographic statistics

Data collection statistics

Space group	$P2_12_12$
Unit cell (Å)	a=141.353, b=178.662, c=95.31, $\alpha=\beta=\gamma=90$
Resolution (Å)	2.0
Reflections	131575
Completeness (%)	92.5
R_{sym} (%)	14.0
$\langle I/\sigma I \rangle$	5.40

Refinement and model statistics

Resolution (Å)	500.0 – 2.0
Reflections in refinement	125215
Cross validation reflections	6660
R_{cryst} (%)	21.54
R_{free} (%)	24.40
Asymmetric unit	3 molecules, ~60 % solvent content
Non-hydrogen atoms	13233
Waters	825
Average B-factor (Å^2)	20.97 overall
	21.203 Monomer A

	22.253 Monomer B
	18.680 Monomer C
	24.730 waters
	33.521 N-acetylglucosamine
Rmsd bond lengths (Å)	0.006
Rmsd bond angles (degrees)	1.29
Ramachandran geometry	88.0 % most favored regions
	11.4 % allowed regions
	0.6 % generously allowed regions
	0.0 % disallowed regions

Table 2. RMSD between five apoenzyme structures of cholesterol esterase (Å)

Structure	Space group	Resolution	2bce	1akn	A	B	C
2bce	C2	1.6 Å	-------	0.998	0.850	0.895	1.251
1akn	$P3_121$	2.8 Å		-------	0.764	0.756	0.887
monomer A	$P2_12_12$	2.0 Å			-------	0.479	0.869
monomer B	$P2_12_12$	2.0 Å				-------	0.895
monomer C	$P2_12_12$	2.0 Å					-------
average rmsd	0.8644 Å						

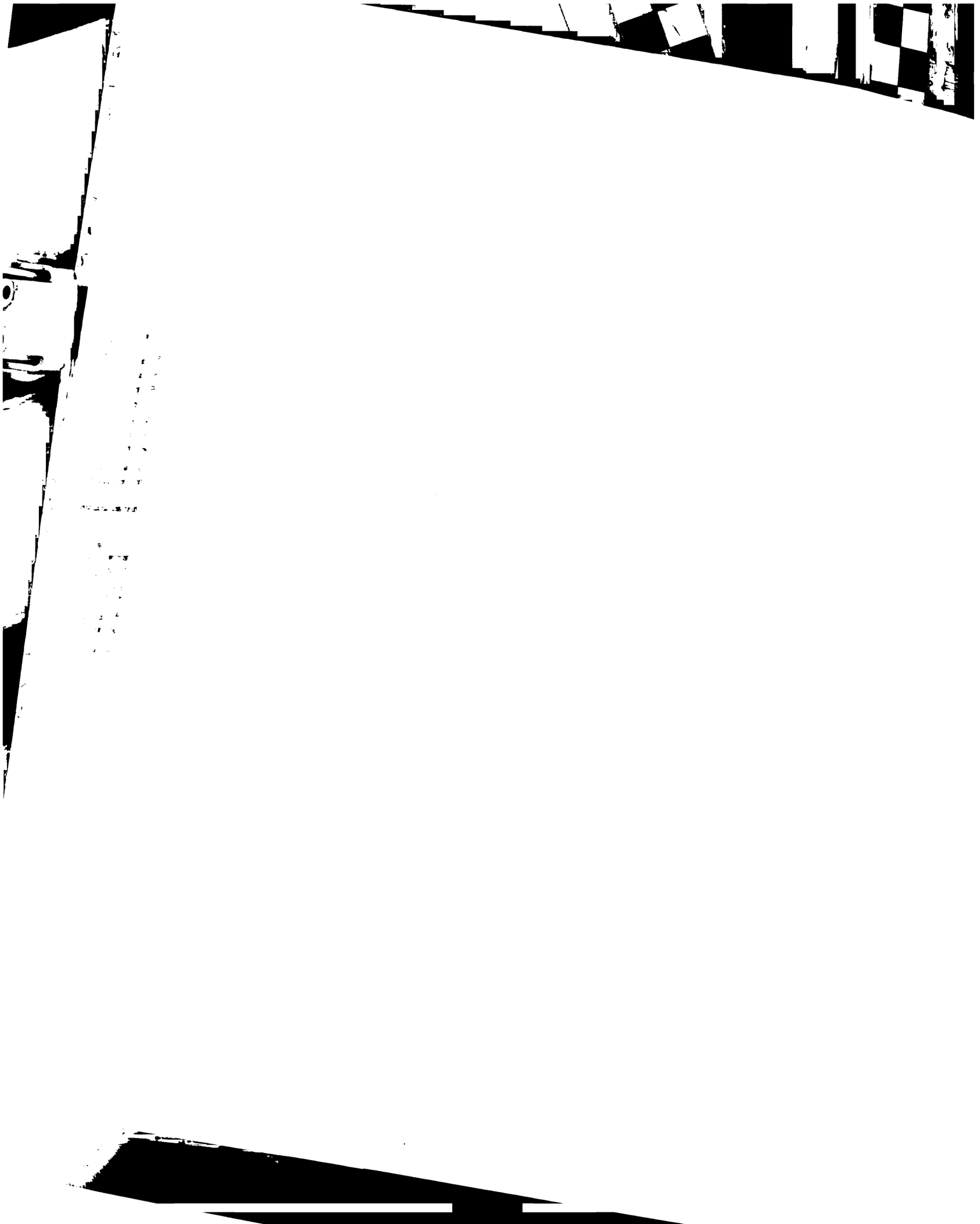

Table 3. Catalytic triad geometry and distances.

Structure	S194 γO-H435 εN (Å)	H435 δN2-D320 O (Å)	S194 γO-D320 O (Å)
Monomer A	2.84	2.70	7.30
Monomer B	2.89	2.84	7.42
Monomer C	3.36	2.78	7.30
1akn	2.90	2.81	7.32
2bce	2.75	3.08	7.46
range	0.61	0.38	0.16

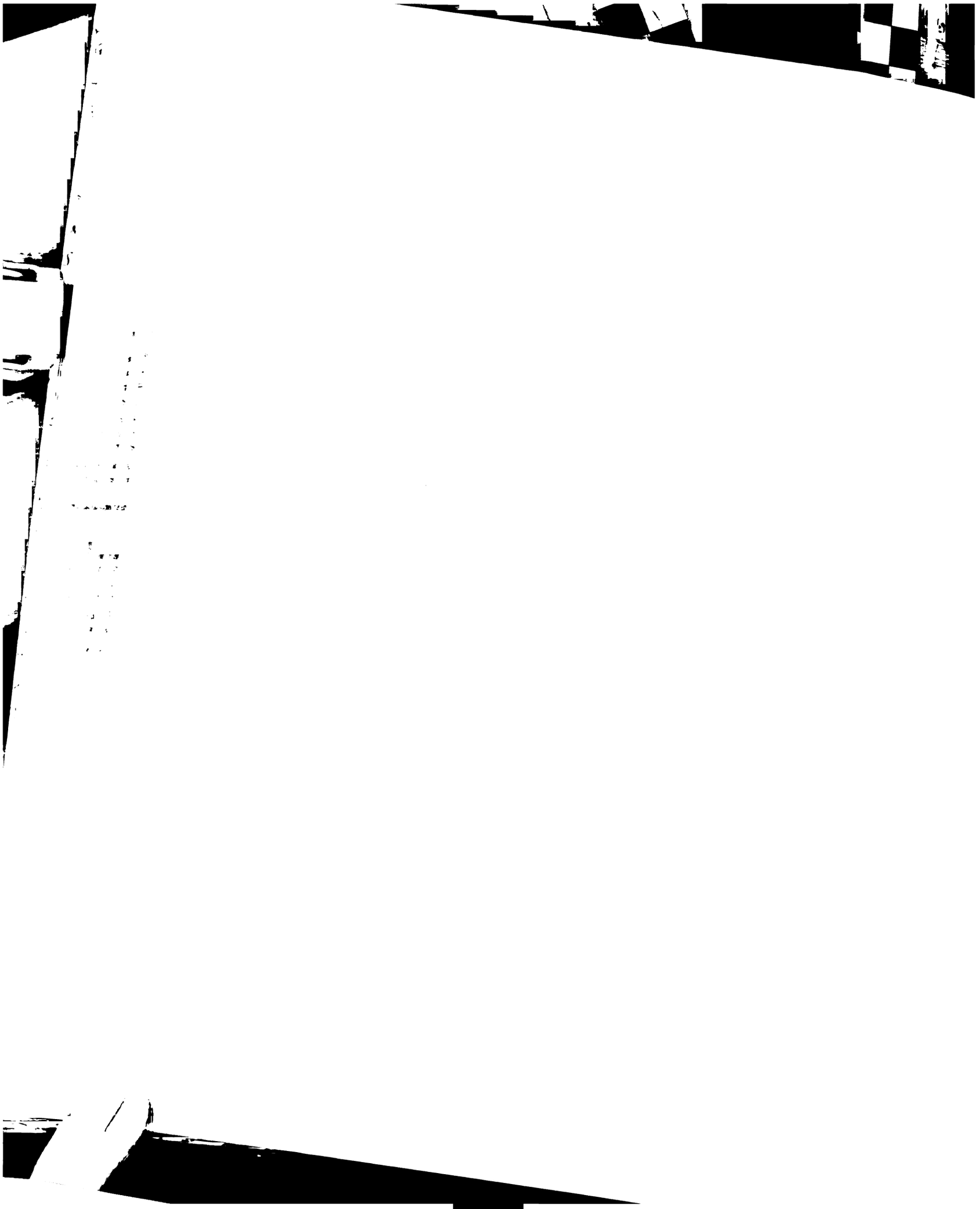

FIGURE LEGENDS

Figure 1: Alpha carbon trace of the asymmetric unit of the $P2_12_12$ form of cholesterol esterase. Monomers are labeled A, B, and C.

Figure 2: $2F_o$-F_c electron density in the catalytic triad region contoured at 1.0 σ. (a) monomer A. (b) monomer B. (c) monomer C. The catalytic εN of His435 is hydrogen bonded to a water molecule, as opposed to the Ser194 hydroxyl seen in the other monomers.

Figure 3: Overlay of the Cα of the five apoenzyme structures (PDB 1akn, 2bce, Monomer A, Monomer B, and Monomer C).

Figure 4: Cα overlay of bile salt loops from the five apoenzyme structures. The bile salt loops adopt significantly different conformations with hinges at Tyr105 and Asp126. Monomers A and B assume an alpha-helical conformation followed by an extended loop.

Figure 5: Cα overlay of the 422-436 loop and 318-390 helical domain. This coupled movement allows catalytic His435 to move into a productive hydrogen bond network with Ser194 and Asp320. The view in (b) is rotated 90 degrees relative to (a). Catalytic residues Ser194, His435, and Asp 320 are highlighted.

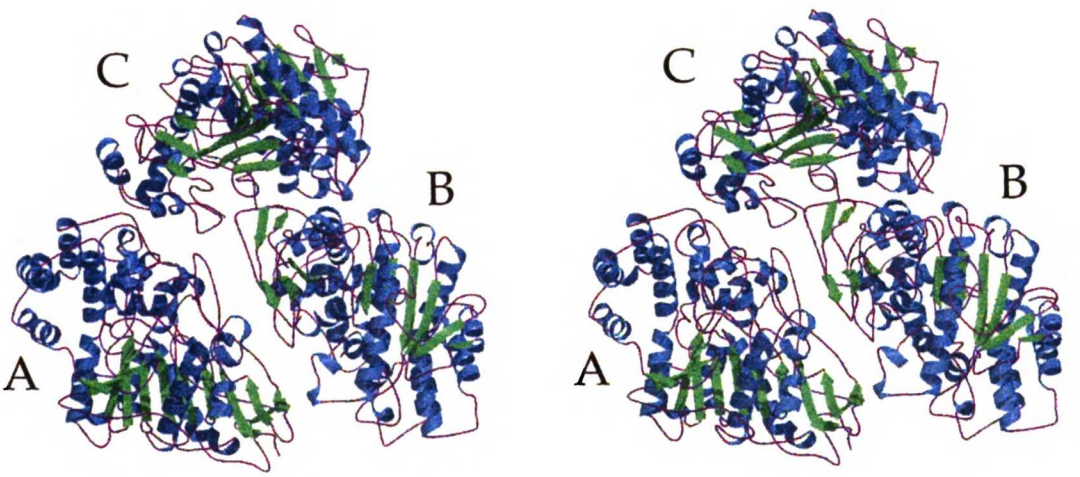

Figure 1.

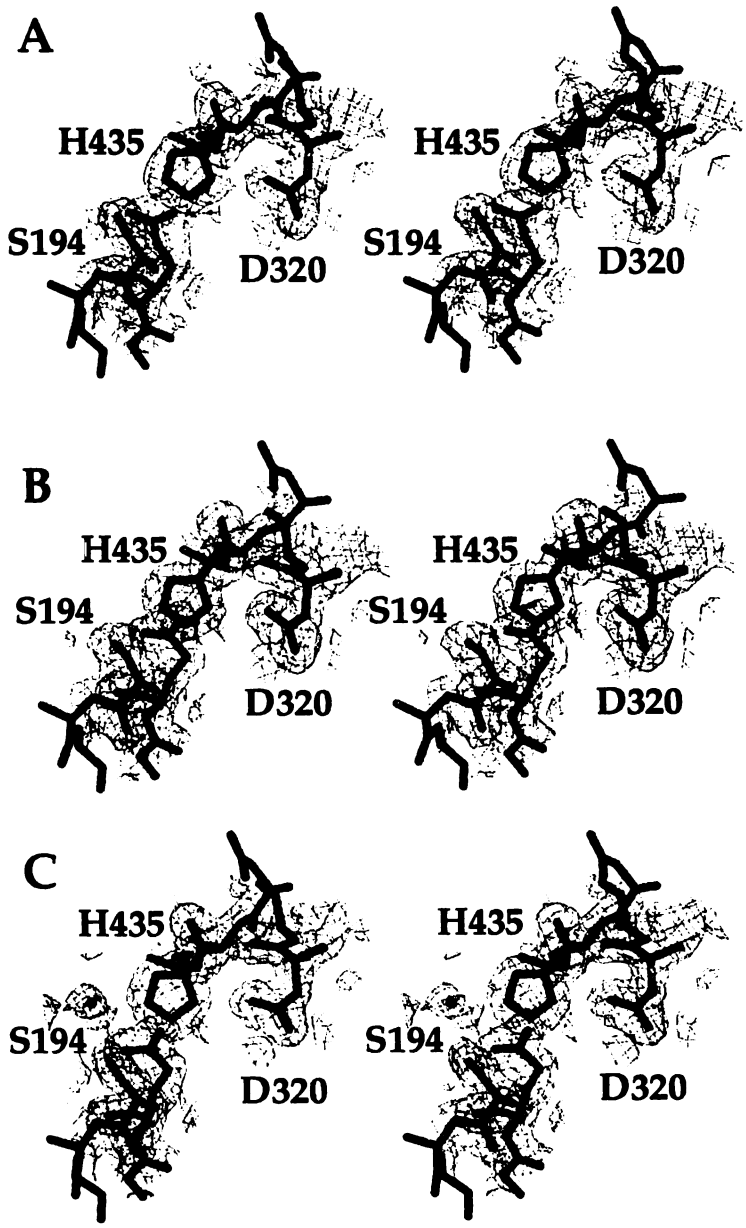
A
H435
S194
D320
H435
S194
D320
B
H435
S194
D320
H435
S194
D320
C
H435
S194
D320
H435
S194
D320

Figure 2.

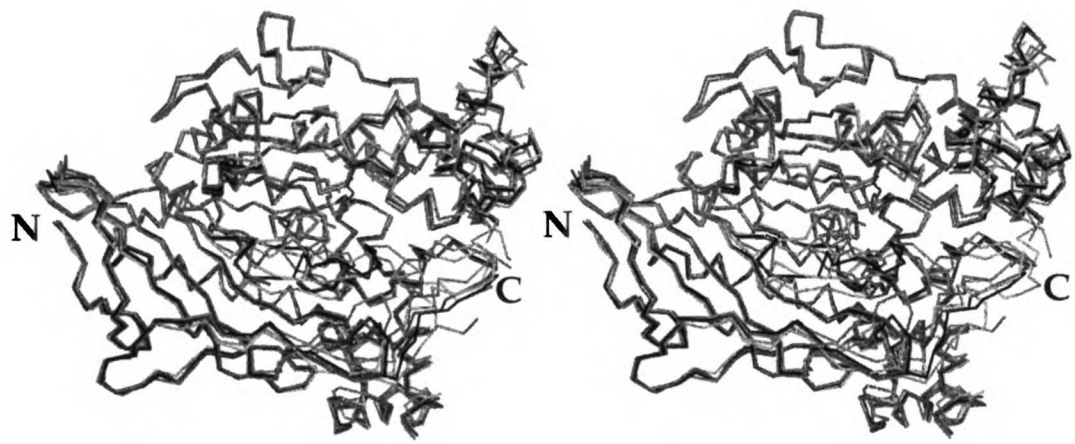

Figure 3.

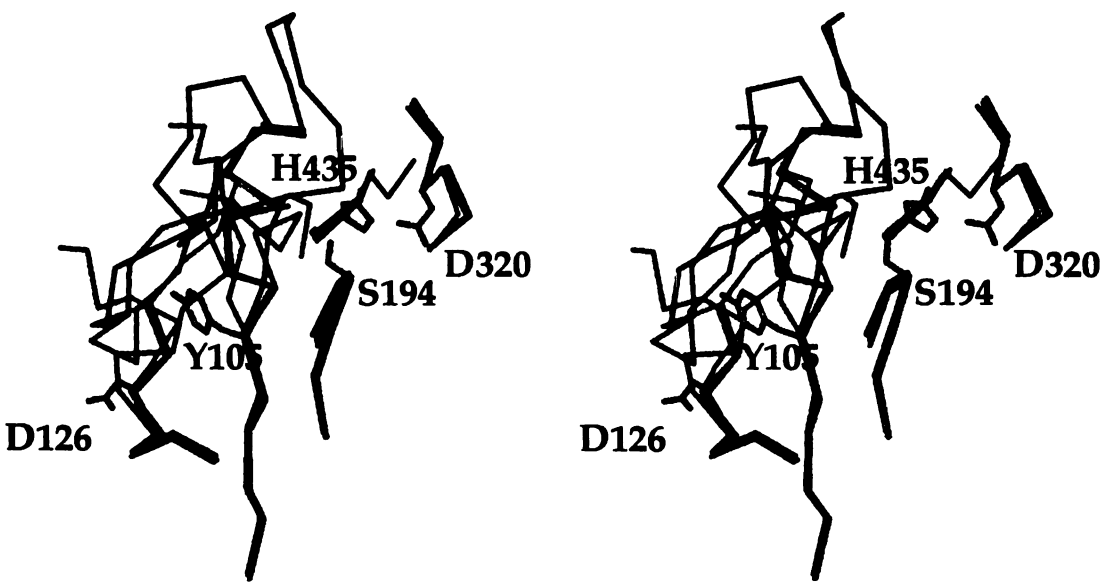

Figure 4.

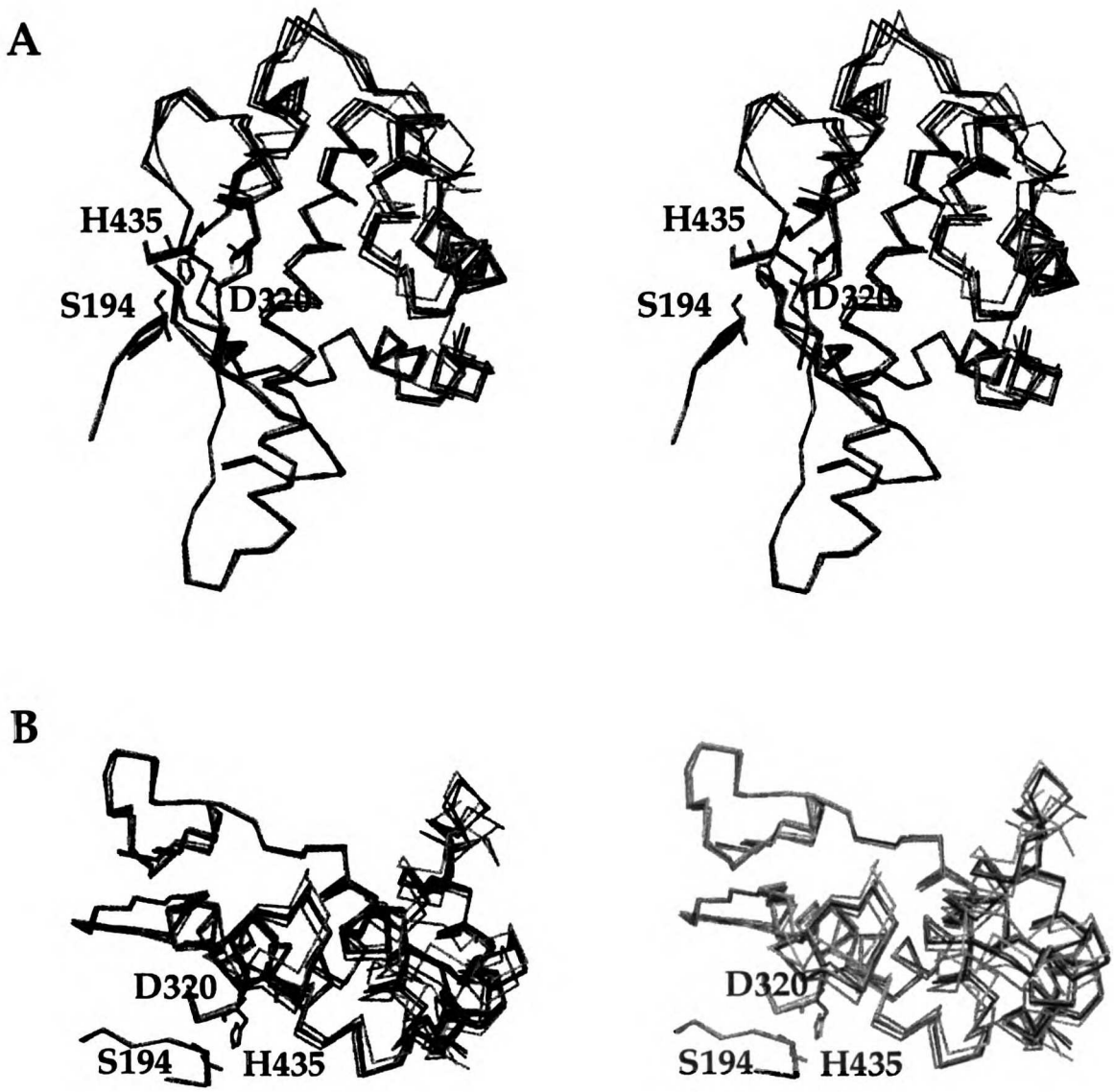
A
H435
S194
D320
H435
S194
D320
B
D320
S194
H435
D320
S194
H435

Figure 5.

Chapter 3

Structure of a pre-activated complex of cholesterol esterase with bile salts

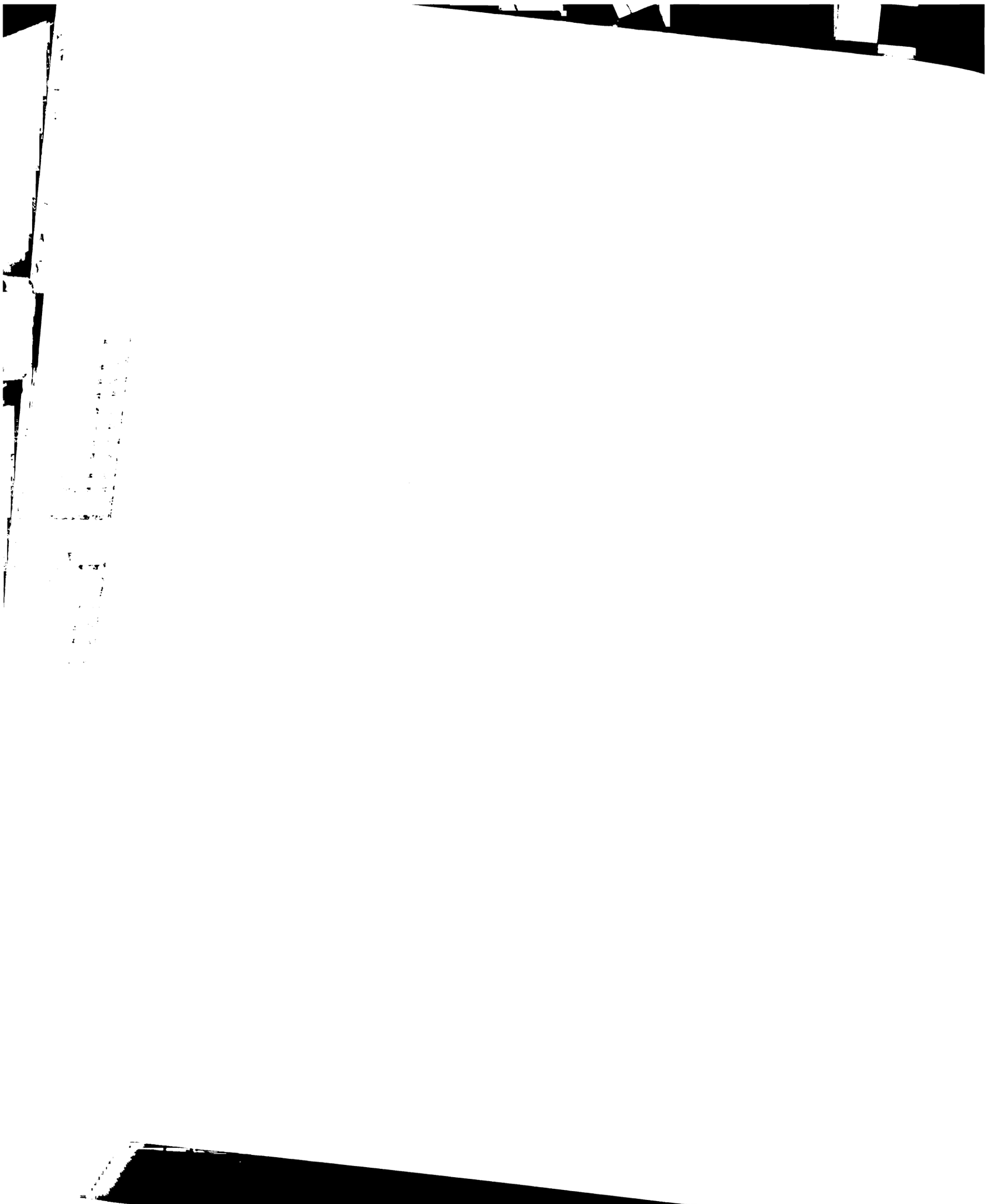

Structure of a pre-activated complex of cholesterol esterase with bile salts

Julian C.-H. Chen, Larry J.W. Miercke, Jolanta Krucinski, and Robert M. Stroud

Graduate Group in Biophysics and Department of Biochemistry and Biophysics, Box 0448, University of California, San Francisco, CA 94143-0448

Running title: Structure of cholesterol esterase bound to bile salts

Coordinates have been deposited in the PDB with code xxxx.

ABBREVIATIONS AND TEXTUAL FOOTNOTES

BSA, bovine serum albumin

PEG, polyethylene glycol

DLS, dynamic light scattering

MES, 2-(*N*-morpholino)ethanesulfonic acid

NCS, non-crystallographic symmetry

CNS, Crystallography and NMR System

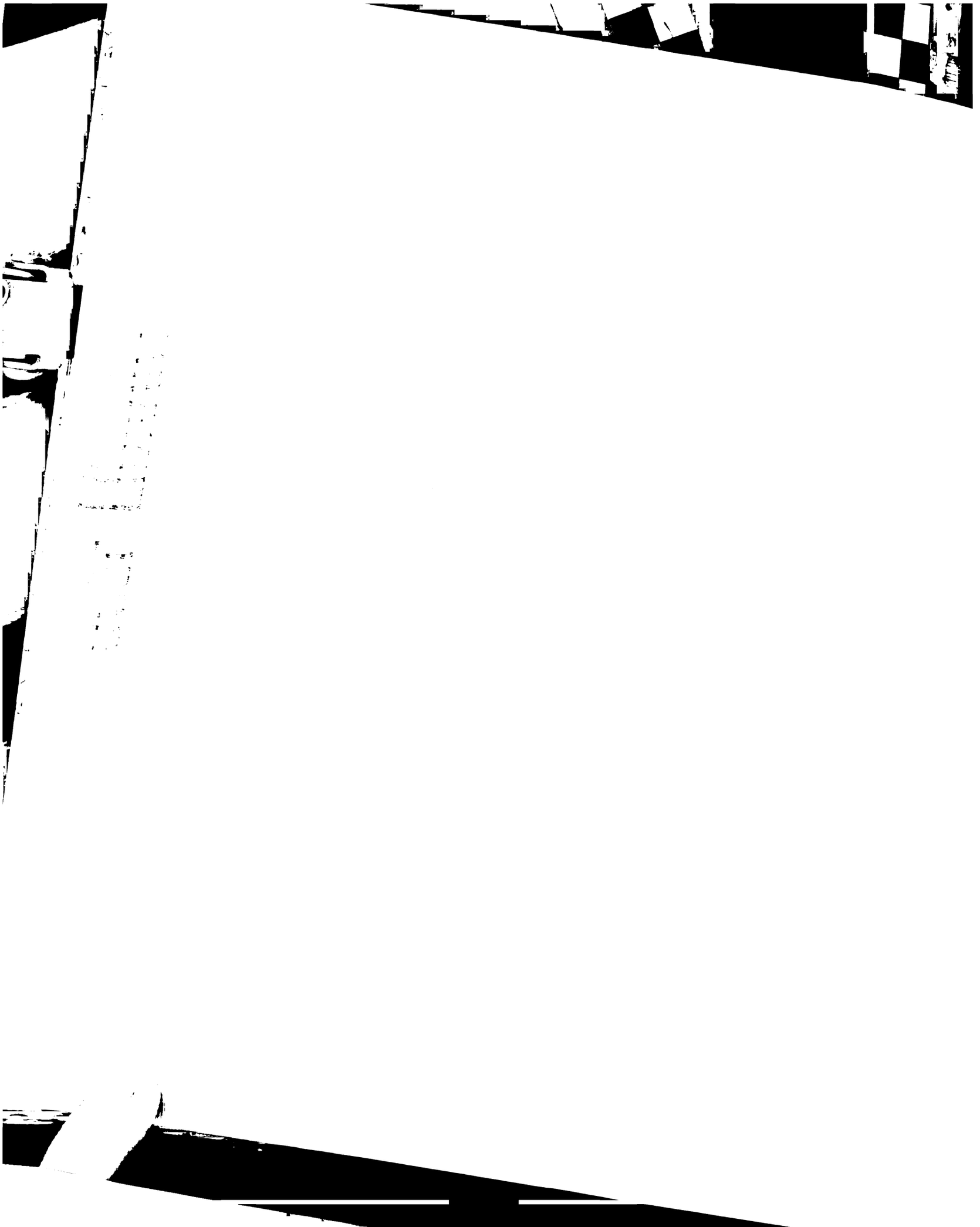

ABSTRACT

The structure of cholesterol esterase, also known as bile salt activated lipase, has been solved in the presence of the activating bile salt taurocholate and the non-activating bile salt taurodeoxycholate. These bile salts differ in the presence of a 7-α hydroxyl group in taurocholate and its absence in taurodeoxycholate. Crystals diffract to 2.0 Å resolution, and the refined structure (R_{free}= 24.2 %, R_{cryst}= 21.0 % for the taurocholate complex, R_{free}= 24.8 %, R_{cryst}= 21.8 % for the taurodeoxycholate complex) shows that one of the three monomers in the asymmetric unit contains bound bile salt. In contrast to an earlier structure crystallized in the presence of taurocholate, only one binding site is occupied by ligand in the present study. Both structures show bile salt bound in the same pocket, a cleft about 10 Å from the active site, and both the activating and non-activating bile salt are bound to cholesterol esterase in the similar conformations. There is little specificity to the interaction, with only one hydrogen bond between the protein and the ligand. However, because only one of the two binding sites on the enzyme contains bile salt, the distal site is of a higher affinity than the activating site, yet it is a nonspecific site. The monomer in the asymmetric unit with a distorted, inactive catalytic triad does not have bound bile salt, however, and we propose that bile salt binding to the distal site on the protein helps order the catalytic triad into a productive conformation, while bile salt binding to the proximal site is involved in lipase activation and enhancement of enzymatic activity.

Cholesterol esterase, also known as bile salt activated lipase, hydrolyzes a wide variety of dietary lipids, from triglycerides to phospholipids, in addition to being the sole digestive tract enzyme responsible for hydrolyzing cholesterol and vitamin esters (1, 2). The low basal activity of cholesterol esterase is significantly enhanced by the addition of bile salts, in contrast to classical lipases, which are activated at an oil-water interface (3).

Activation of cholesterol esterase is absolutely dependent on the presence of a 7-α hydroxyl group on the bile salt, therefore in order to understand this exquisite discrimination among bile salts, we grew crystals of cholesterol esterase in the presence of the activating bile salt taurocholate and the non-activating bile salt taurodeoxycholate. Taurocholate contains 3-, 7-, and 12-α hydroxyl groups, while taurodeoxycholate contains the 3- and 12-α hydroxyl group, and lacks the 7-α hydroxyl (Figure 1). We crystallized native cholesterol esterase in the presence of saturating concentrations of bile salts and also in the absence of bile salts. Both grew under nearly identical conditions, and we report structures of the two complexes of cholesterol esterase with bile salts. In both structures, we find one binding site for bile salt occupied, that of the distal site reported in the structure of Wang, et al (4). This distal binding site is occupied by both the activating and non-activating bile salt, while the proximal, activating site containing the bile salt loop (residues Tyr105-Asp126) is unoccupied. Therefore we have isolated a pre-activated complex of cholesterol esterase with bile salt. We propose from the structures that the purpose of bile salt binding to the distal site may be to order the catalytic triad in a productive orientation for activity, as

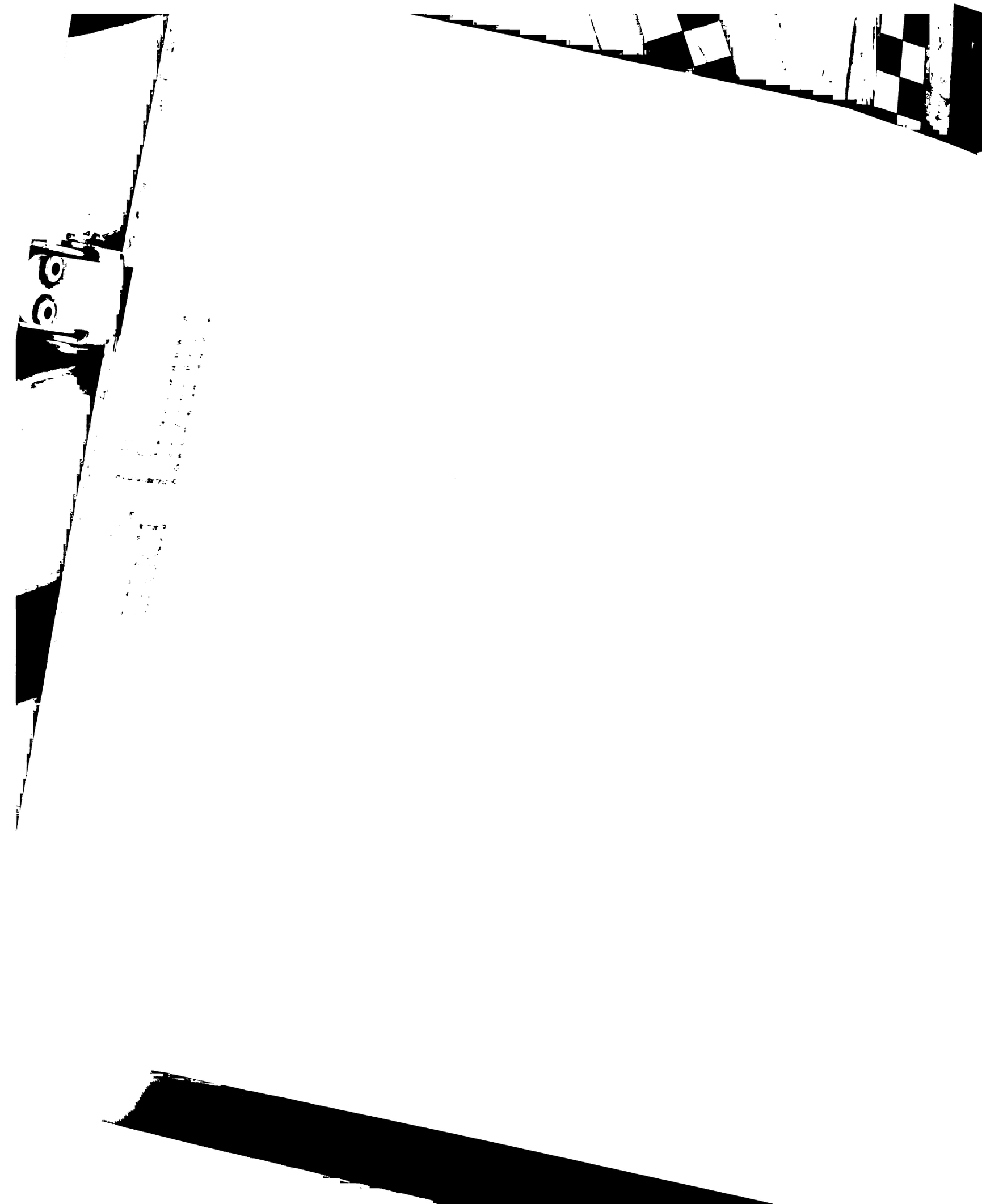

bile salt is bound in only one monomer in the asymmetric unit. Interestingly, the distal site appears to be of higher affinity than the activating site, in spite of the lack of specificity.

MATERIALS AND METHODS

Purification. .Native wild-type CEase from bovine pancreas was purified on S-sepharose and SP-sephadex columns according to a previously published protocol (5) with one additional step. The pooled fraction from SP-sephadex was concentrated, and dialyzed overnight against 20 mM MES pH 6.0, 50 mM NaCl. The dialyzed target was filtered and injected into a 1.2 cm x 10 cm Poros HS strong cation exchanger (Perseptive Biosystems) run at 4 ml/min in 20mM MES pH 6.0. At 1 minute post injection, a 5 minute 0 M to 0.45 M NaCl gradient was run with target elution at ~30% NaCl.

Molecular size characterization. The hydrodynamic stoichiometry and molecular weight were assessed using the DynoPro-801 Dynamic Light Scattering/Molecular Sizing Instrument equipped with a micro-cuvette based MicroSampler (Protein Solutions) based on a previously described protocol (6). Measurements were performed on a sample concentrated to 2 mg/ml and buffered with Na-acetate pH 5.0 and 50 mM NaCl with 1.5 and 3.0 mM taurocholate.

Crystallization. Purified native wild-type CEase was concentrated to approximately 5 ml, dialyzed 48 hours against 2 L 25 mM Na-acetate pH 5.1 and 100 mM NaCl. The protein was further concentrated to 5-6 mg/mL for

crystallization trials. Protein concentration was determined by the Bradford assay using bovine serum albumin (BSA) as a standard.

Crystals of native CEase in complex with taurocholate were grown at room temperature by vapor diffusion using PEG 3000 as precipitant with Na/K-phosphate as an additive. Native CEase at 7 mg/mL in Na-acetate pH 5.1, 100 mM NaCl were mixed with equal volumes of a reservoir solution containing 20 % PEG 3000, 80 mM buffer pH 5.9-6.5, 150 mM Na/K phosphate and 1-3 mM taurocholate. Crystals typically appeared in 2-3 days and were of similar quality and morphology as that of the native CEase apoenzyme. Subsequently, crystals of CEase in complex with taurodeoxycholate were grown in a similar manner.

Data collection. Data were collected at Stanford Synchotron Radiation Laboratory Beamline 7-1 (λ=1.08 Å) on a 30 cm image plate (MAR Research). Crystals were transferred quickly from the drop to a 7 µl solution of cryosolvent composed of 25 % PEG 3000, 80 mM Na-citrate pH 6.5, 50 mM NaCl and 0.2 M ammonium sulfate or Na-phosphate solution containing 20 % glycerol as a cryoprotectant. Crystals were then flash frozen in a nitrogen gas stream at 90 K. Data were indexed, integrated, and scaled using DENZO/SCALEPACK (7) using with no σ cutoff. The taurocholate/CEase crystal indexed in space group $P2_12_12$ with cell dimensions a=141.326 Å, b=177.956 Å, c=95.28 Å, $\alpha=\beta=\gamma=90$. The taurodeoxycholate/CEase crystal indexed in the same space group with slightly altered cell dimensions: a=141.486 Å, b=178.551 Å, c=95.445 Å, $\alpha=\beta=\gamma=90$. A 5 % set of reflections between 500 and 2.0 Å resolution in the two datasets was set aside prior to refinement for calculating R_{free} (8, 9).

Structure solution and refinement. A calculation of the Matthews coefficient revealed a possible 2-5 monomers per asymmetric unit. A truncated model of the apoenzyme structure of Chen, et al. (PDB code 2bce) was used as a search model against the taurocholate/cholesterol esterase dataset (6). The truncated model was constructed based on a least-squares alignment of the apoenzyme structures of Wang, et al. (4) and Chen, et al. (PDB code 1akn and 2bce) in LSQMAN, with all residues showing > 1.5 Å root mean square deviation (rmsd) in their respective Cα positions deleted from the model (4). Using this model, a rotation and translation search in AMoRe resulted in a solution with 51 % R-factor (10). This solution was rigid-body refined and fixed to find additional molecules in the asymmetric unit. Two additional molecules were located, with an initial R-factor of 39 % after refinement of all three molecules. Attempts to find additional monomers in the asymmetric unit resulted in an increased R-factor and lowered correlation coefficient. The solvent content was approximately 60 %. Initial non-crystallographic symmetry (NCS) restraints were used in the early stages of refinement to maximize the data to parameters ratio, along with the use of averaged maps for building. However, it was evident that there were significant differences in the structures of the three monomers, so NCS restraints were dropped after the first round of refinement and the molecules were built separately. CHAIN (11) was used for model building throughout, and XPLOR (12) and CNS (Crystallography and NMR System) (13-15) were used for refinement. CNS utilizes a maximum likelihood target function, and all data collected were used in refinement. A bulk solvent correction was applied throughout refinement. A combination of positional, individual temperature

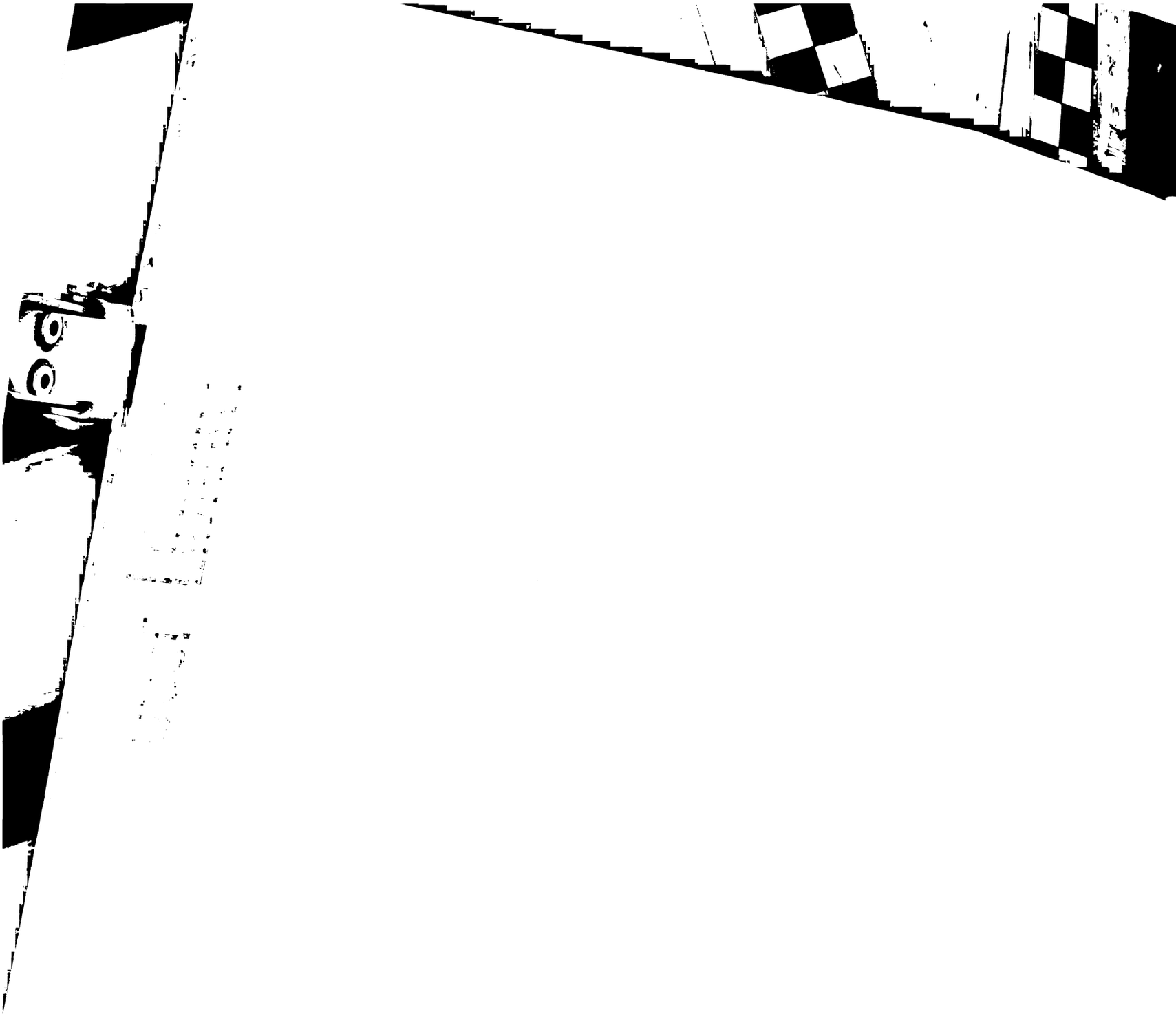

factor, and simulated annealing refinement was used to lower the R_{free} to 24.22 % and the R_{cryst} to 20.99 % (16).

Subsequently, this model was used to solve the taurodeoxycholate structure, with a difference F_o-F_c map calculated with water molecules and taurocholate eliminated from the model. The starting R-factor was 31 %, and rounds of positional, temperature factor, and simulated annealing refinement in CNS reduced the R_{free} to 24.7 % and the R_{cryst} to 21.7 % (16). Simulated annealing omit maps were calculated to confirm the modeling of taurocholate and taurodeoxycholate in the two structures. Statistics of data collection and refinement are presented in Table 1. Structural alignments were done using LSQMAN, an O utility (17). Figures were generated using MOLSCRIPT (18) and Raster3D (19).

RESULTS AND DISCUSSION

Solution stoichiometry. Dynamic light scattering (DLS) was run on native bovine pancreatic cholesterol esterase in the presence of 1.5 and 3.0 mM taurocholate (Figure 1). Two independent runs clearly indicated the presence of only one scattering population corresponding to the monomeric species with a molecular weight of 63 kD, in agreement with the calculated molecular weight of 63.5 kD. The polydispersity index was less than 6 % of the mean value of the hydrodynamic radius. This indicates that the enzyme does not dimerize in the presence of bile salt, as suggested by the structure of Wang, et al (4). The earlier apoenzyme structure of Chen, et al. shows a monomeric species of the native

unliganded enzyme (6). This is in contrast to the cholesterol esterase of *Candida cylindracea*, which shows a significant buried surface area upon dimerization and is thought to be important for the function of the protein (20).

Crystal structures. Crystals grew in space group $P2_12_12$, with three molecules per asymmetric unit. The structures of the individual monomers follow the basic fold of the α–β hydrolase family. However, a detailed examination of the three structures reveals significant differences between them. We present these results and their implications in the accompanying structure of the unliganded cholesterol esterase in the same space group (Chen, et al., previous chapter). In brief, the asymmetric unit of the unit cell is composed of three monomers of cholesterol esterase, Monomers A, B, and C, of which Monomers A and B are similar in respect to their overall rmsd among their Cα positions and the conformation of their bile salt loops. Monomer C, which contacts Monomer A extensively and Monomer B less so, is considerably different. While the overall architecture and fold of Monomer C remain the same, there are significant differences in the conformation of the bile salt loop and the active site catalytic triad. The bile salt loop is displaced 90 degrees relative to the conformations in Monomers A and B, and the catalytic triad contains a displaced His435, such that the hydrogen bond to the εN is satisfied by a water molecule instead of the serine hydroxyl.

Bile salt binding. The ligand, taurocholate, an activating bile salt, is clearly seen in only one of the three monomers, that of Monomer B. There is poor electron density in Monomer A at the site of the ligand that was not modeled and there was no discernable electron density for the ligand in Monomer C. Only one

bile salt binding site is occupied in Monomer B, in contrast to the structure of Wang, et al., which shows two bile salt binding sites per protein monomer. The taurocholate is modeled into the distal site. In the structure of cholesterol esterase with taurodeoxycholate, the non-activating bile salt occupies the same cleft in an analogous manner, and is only seen in good density in Monomer B. Both molecules are bound in a similar conformation, with few specific contacts between the bile salt and the protein. There is only one specific interaction, a hydrogen bond between the εN2 of Gln527 and the 12-α hydroxyl of the bile salts (Figure 4). In the crystal, there is a second hydrogen bond between the 3-α hydroxyl of the bile salts and a symmetry related εN2 from Gln524 but may not be physiologically relevant, as cholesterol esterase bound to taurocholate is monomeric in solution. Van der Waals contacts determine the bulk of the protein-ligand interaction.

In contrast to the structure of Wang, et al., the alkyl tail of the bile salt is relatively disordered, with higher temperature factors (>60 $Å^2$) and poor electron density for the electron-rich sulfate group. The placement is equivocal, indicative of flexibility in the alkyl tail.

The bile salt loop is in a 'closed' conformation in all three monomers. In spite of co-crystallization with saturating and/or near-saturating concentrations of bile salt (3-9 x K_d), a possible explanation for this is incomplete reaction of the bile salt with the protein in the crystallization mixture combined with the weak K_d(~400 μM) of the bile salt for cholesterol esterase. While Wang, et al. was able to crystallographically visualize an activated conformation of the taurocholate/cholesterol esterase complex, we have visualized a pre-activated

complex of the enzyme. We propose that binding of bile salt to this distal site may shift the equilibrium of conformations towards ones with competent active sites, i.e. catalytic triad residues in good hydrogen bonding distance and geometry with one another. The presence of bile salt at the distal site and not the proximal site implies that the binding of bile salt to distal site may be of a higher affinity. Conformational changes to the protein upon binding this distal site are minimal, with a rmsd between the unliganded Monomer B and the liganded Monomer B of 0.346 Å in the case of taurocholate and 0.371 Å in the case of taurodeoxycholate. Also, the lack of bile salt seen in Monomer C implies that bile salt may 'select' for productive active site conformations, as Monomer C does not have a productive catalytic triad.

Ironically, because both taurocholate and taurodeoxycholate bind to the same site, the distal binding site may not only be of higher affinity than the proximal, activating site, but is also nonspecific, a rather contradictory occurrence as specificity is typically associated with higher affinity. It is also important to note that the binding of bile salts to the distal site seen in this structure does not appear to influence the binding of bile salts to the proximal site. We conclude that these bile salt sites are independent and that there is no cooperativity present in the context of binding. In the context of enzymatic activity and function, however, we propose that binding of bile salt to the distal site is necessary for activity, and therefore these sites are allosteric.

We have located a nonspecific binding site for bile salts in the enzyme cholesterol esterase. The binding modes of taurocholate and taurodeoxycholate are very similar, occupying a cleft in the enzyme between a primarily helical

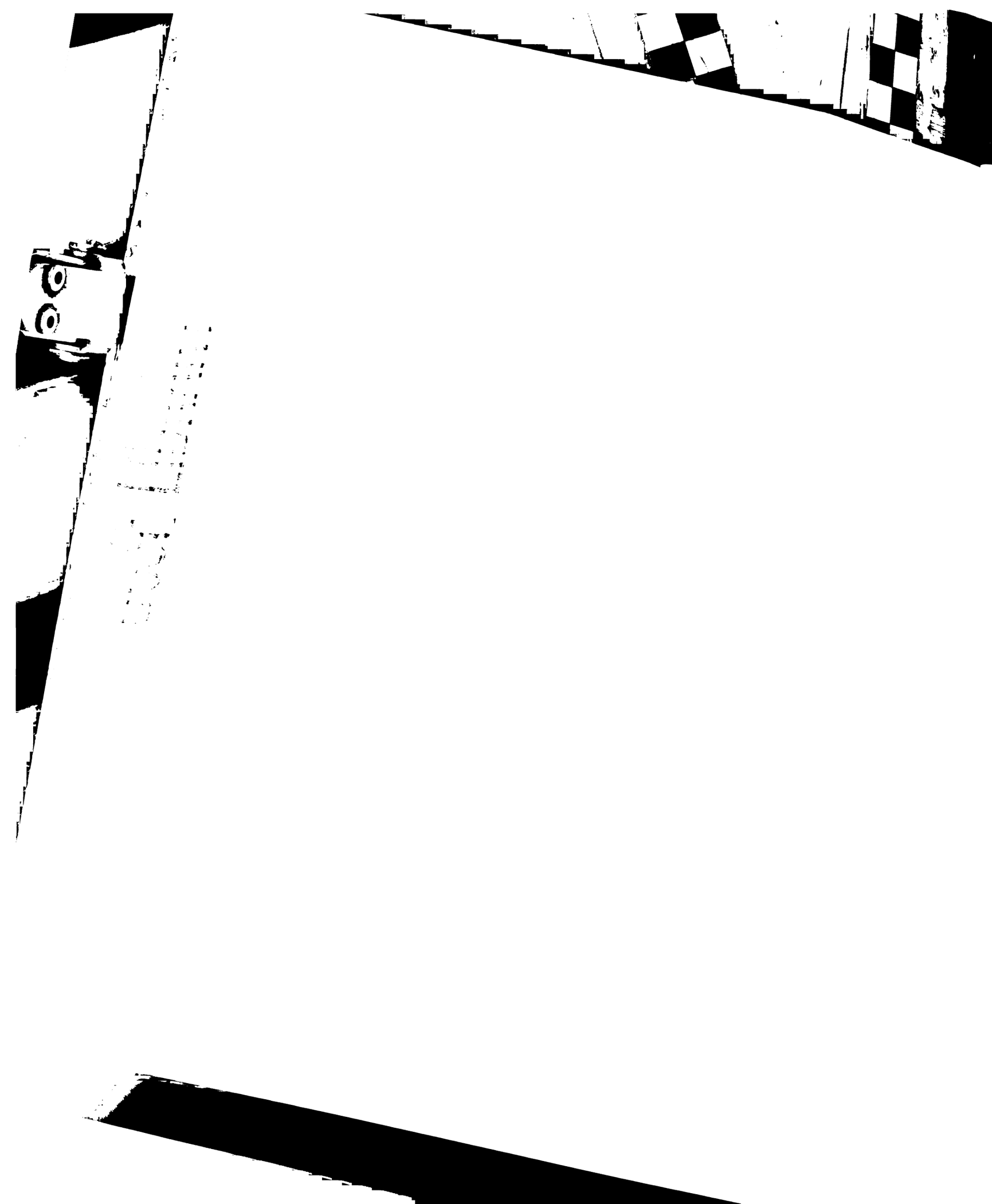

domain and a mixed alpha-beta core. This is consistent with the structure of Wang, et al., which showed two bile salt binding sites.

There have been biochemical studies showing at least one bile salt binding site, a site distinct from the activating site (21, 22). The structural results presented here are in agreement with the notion of distinct bile salt binding sites.

The binding of taurocholate and taurodeoxycholate in the distal site appears to be independent of the site responsible for activation and enhancement of enzymatic activity. The principal determinants of binding are complementarity of the van der Waals surfaces of the bile salt and the binding site, in addition to hydrogen bonding between the available hydroxyl groups of the bile salts and the protein.

These results indicate that cholesterol esterase can assume a variety of different conformations. In the unliganded forms of the enzyme, two of the three molecules of the asymmetric unit are in significantly different conformations. However, the molecule containing liganded taurocholate (monomer B) is in a very similar conformation to unliganded monomer B, indicating that very little conformational change is conferred upon bile salt binding.

ACKNOWLEDGMENTS

We thank Drs. Tim Fritz, Amy Anderson and Janet Finer-Moore for helpful comments and discussion and Xingbo Wang (CV Therapeutics, Inc.) for providing protein.

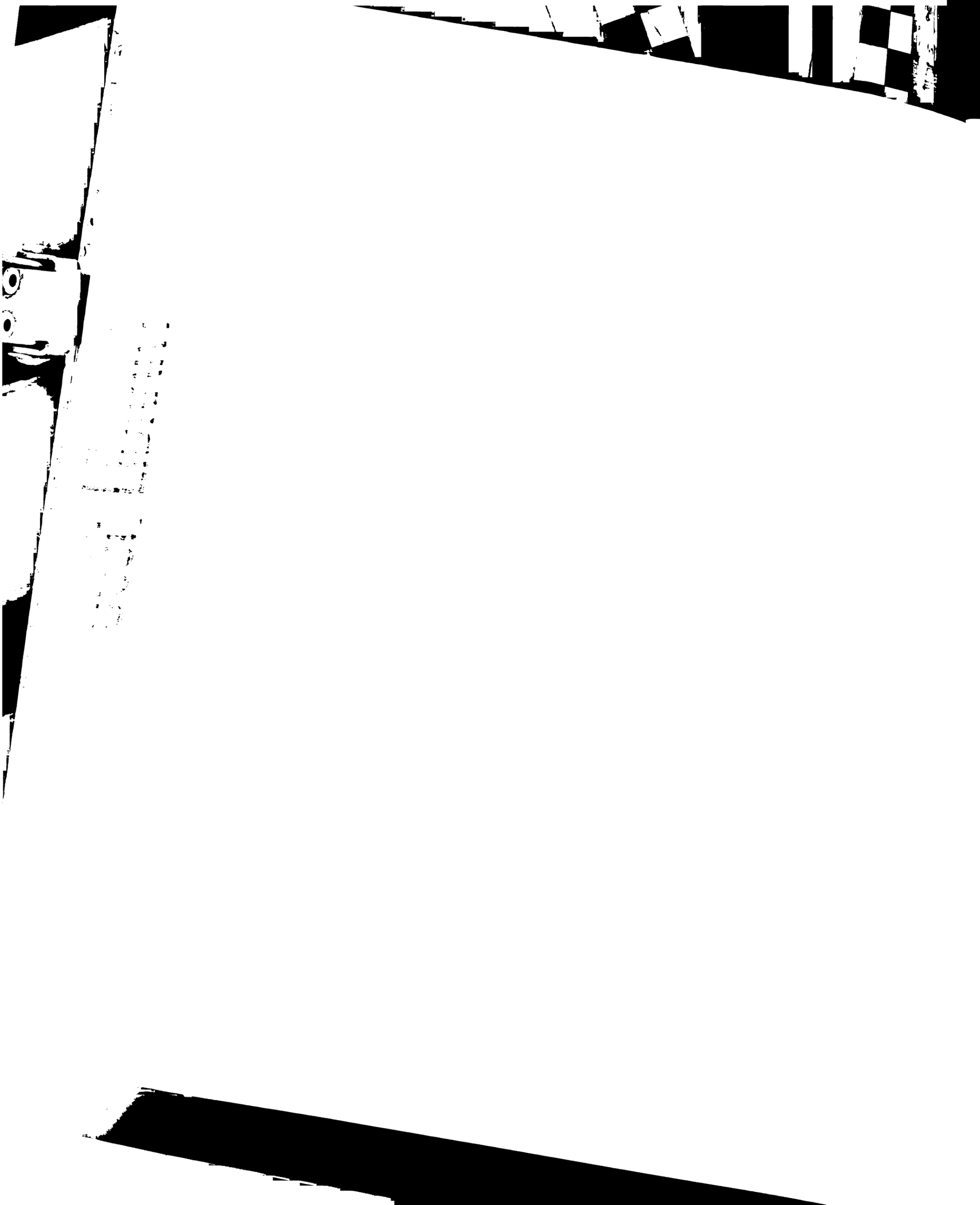

REFERENCES

1. Wang, C. S., & Hartsuck, J. A. (1993) *Biochem. Biophys. Acta 1166*, 1-19.

2. Hui, D. Y. (1996) *Biochem. Biophys. Acta 1303*, 1-14.

3. Rubin, B. (1994) *Nat Struct Biol 1*, 568-72.

4. Wang, X., Wang, C.-S., Tang, J., Dyda, F., & Zhang, X. C. (1997) *Structure 5*, 1209-1218.

5. Spilburg, C. A., Cox, D. G., Wang, X., Bernat, B. A., Bosner, M. S., & Lange, L. G. (1995) *Biochemistry 34*, 15532-8.

6. Chen, J. C.-H., Miercke, L.J.W., Krucinski, J., Starr, J.R., Saenz, G., Wang, X., Spilburg, C.A., Lange, L.G., Ellsworth, J.L., and Stroud, R.M. (1998) *Biochemistry 37*, 5107-5117.

7. Otwinowski, Z. (1993) in *Data Collection and Processing* (Sawyer, L., Isaacs, N. W., & Bailey, S., Eds.) pp 556-562, SERC Daresbury Laboratory, Warrington.

8. Brunger, A. T. (1992) *Nature 355*, 472-475.

9. Kleywegt, G. J., & Brunger, A. T. (1996) *Structure 4*, 897-904.

10. Navaza, J. (1994) *Acta Cryst. A50*, 157-63.

11. Sack, J. S. (1988) *J. Mol. Graphics 6*, 224-225.

12. Brunger, A. T. (1992) *X-PLOR: A System for X-Ray Crystallography and NMR*, Yale Univ. Press, New Haven.

13. Brunger, A. T., Adams, P. D., Clore, G. M., DeLano, W. L., Gros, P., Grosse-Kunstleve, R. W., Kuszewski, J., Nilges, M., Pannu, N. S., Read, R. J., Rice, L. M., Simonson, T., & Warren, G. L. (1998) *Acta Crystallogr. D Biol. Crystallogr. 54*, 905-921.

14. Adams, P. D., Pannu, N. S., Read, R. J., & Brunger, A. T. (1997) *Proc. Natl. Acad. Sci. 94*, 5018-5023.

15. Pannu, N. S., & Read, R. J. (1996) *Acta Crystallogr. A 52*, 659-668.

16. Brunger, A. T., Adams, P. D., & Rice, L. M. (1997) *Structure 5*, 325-36.

17. Jones, T. A., Zou, J. Y., Cowan, S. W., & Kjeldgaard, M. (1991) *Acta Crystallogr. A 47*, 110-9.

18. Kraulis, P. J. (1991) *J. Appl. Crystallogr. 24*, 946-50.

19. Merritt, E. A., & Murphy, M. E. P. (1994) *Acta Cryst. D50*, 869-73.

20. Ghosh, D., Wawrzak, Z., Pletnev, V. Z., Li, N., Kaiser, R., Pangborn, W., Jornvall, H., Erman, M., & Duax, W. L. (1995) *Structure 3*, 279-88.

21. Tsujita, T., Mizuno, N.K., and Brockman, H.L. (1987) *J. Lipid Res. 28*, 1434-1443.

22. Blackberg, L., & Hernell, O. (1993) *FEBS Lett. 323*, 207-210.

Table 1. Crystallographic statistics

Crystallographic and refinement statistics

Ligand	taurocholate	taurodeoxycholate
Unit cell (Å)	a=141.326	a=141.486
	b=177.956	b=178.551
	c=95.280	c=95.445
	$\alpha=\beta=\gamma=90$	$\alpha=\beta=\gamma=90$
Space group	$P2_12_12$	$P2_12_12$
Resolution	2.0 Å	2.0 Å
Completeness (%)	93.3	95.5
$<I/\sigma I>$	9.8	7.4
Reflections > 2.0 σ	135687	135541
R_{sym} (%)	11.4	14.0
Protein atoms	12263	12277
Waters	815	778
<B> overall ($Å^2$)	26.258	22.438
<B> ligand ($Å^2$)	52.818	48.465
Rmsd bond angles (deg)	1.31287	1.30916
Rmsd bond lengths (Å)	0.007	0.006
R_{free} (%)	24.22	24.77
R_{cryst} (%)	20.99	21.75
Ramachandran	87.7 % core	88.2 % core

11.1 % allowed	11.1 % allowed
1.0 % generously allowed	0.7 % generously allowed
0.2 % disallowed	0.0 % disallowed

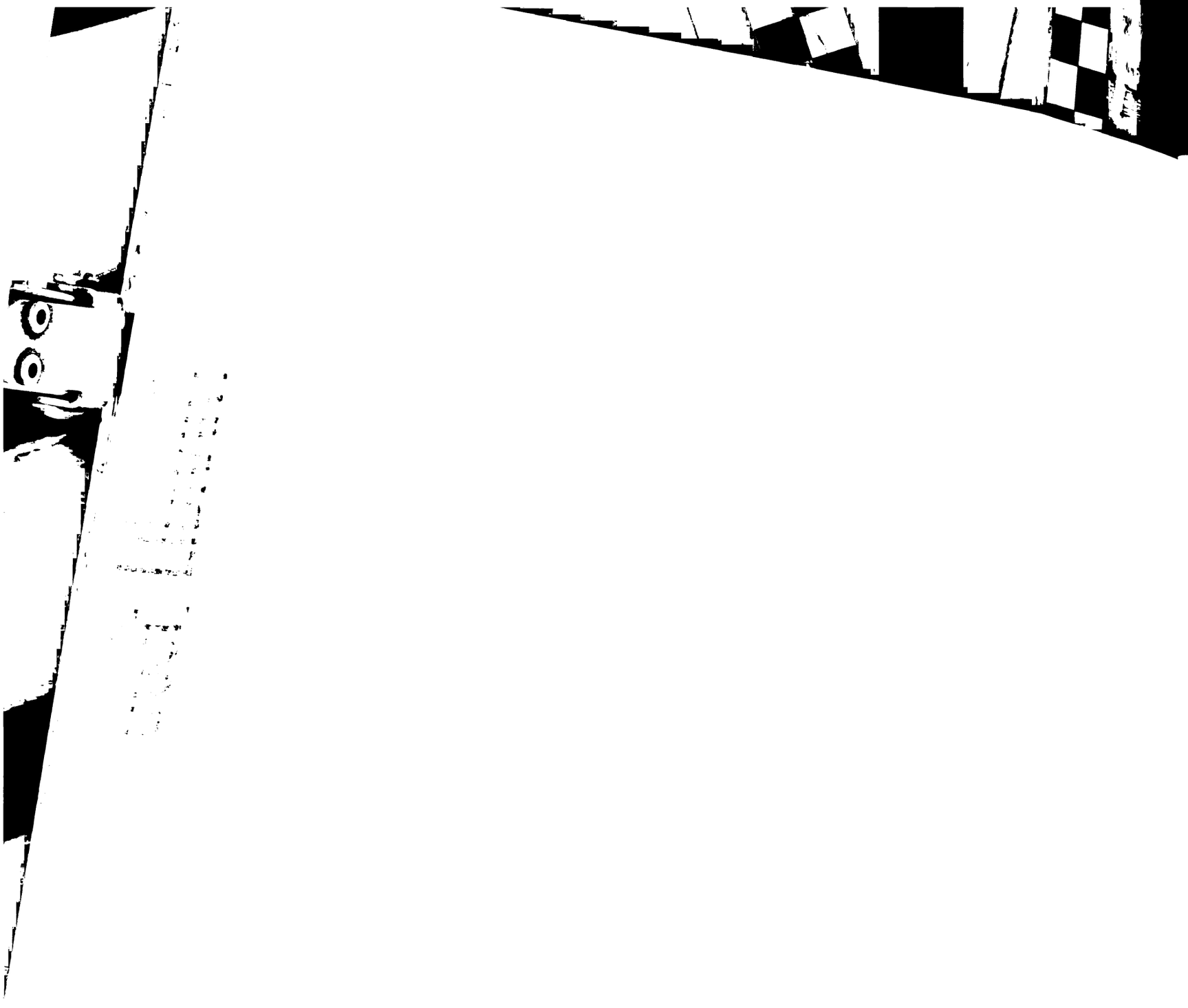

FIGURE LEGENDS

Figure 1: Structures of (a) taurocholate and (b) taurodeoxycholate. Taurodeoxycholate lacks the 7-α hydroxyl group necessary for activation of cholesterol esterase.

Figure 2: Arrangement of monomers in the asymmetric unit of the $P2_12_12$ form of cholesterol esterase. Monomers are labeled A, B, and C.

Figure 3: Overview of the distal bile salt binding site of cholesterol esterase. Active site residues Ser194, His435, and Asp320 are shown in ball-and-stick representation. Bile salt occupies a cleft between an alpha-helical domain of the protein and the catalytic core.

Figure 4: Simulated annealing omit maps of (a) taurocholate and (b) taurodeoxycholate. F_o-F_c maps were created by omitting the ligand from the structure factor calculation and doing a low temperature (1000 K) simulated annealing on the remainder of the asymmetric unit. Map is contoured at 2.5 σ. The single specific interaction between the bile salts and the protein is a hydrogen bond between the εN2 of Gln 527 and the 12-α hydroxyl of the bile salts.

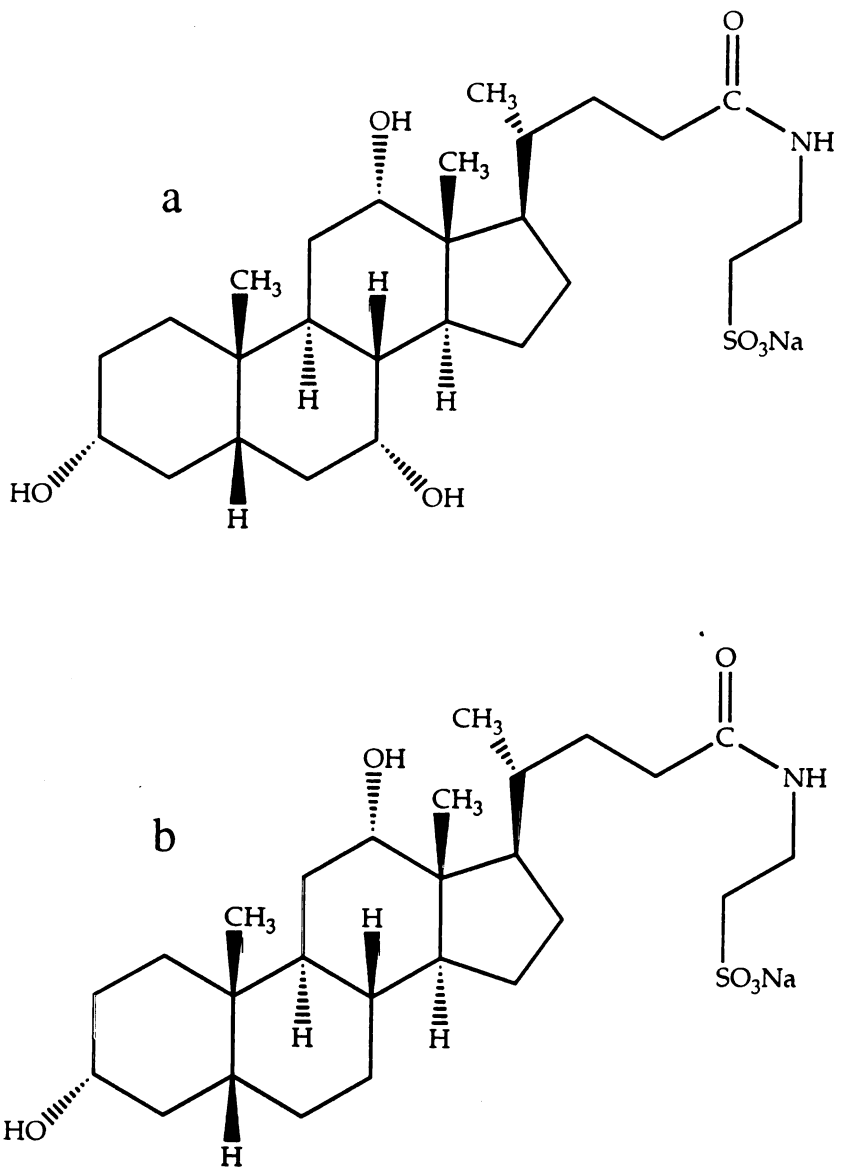
a
O
C
NH
CH3
OH
CH3
CH3
H
SO3Na
H
H
HO
OH
H
b
O
C
NH
CH3
OH
CH3
CH3
H
SO3Na
H
H
HO
H

Figure 1.

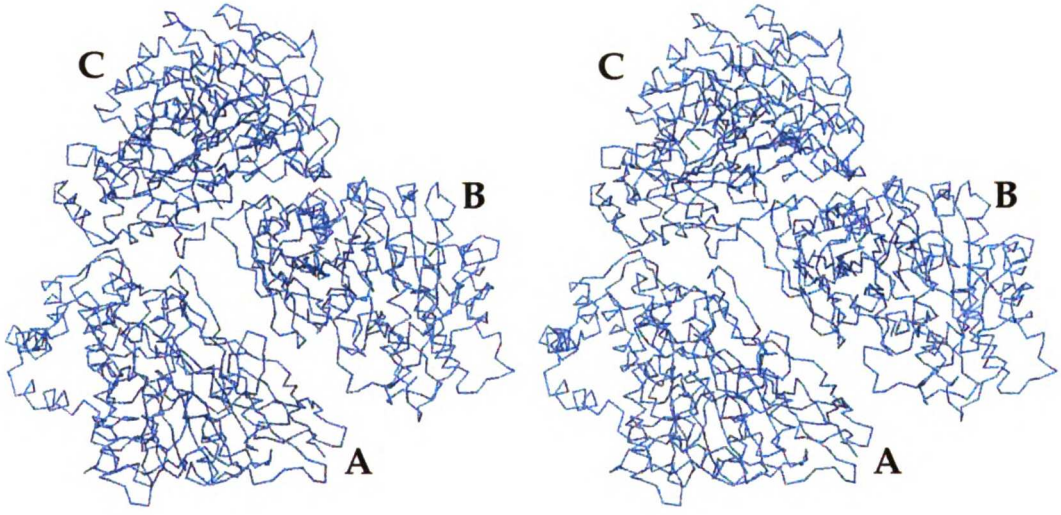

Figure 2.

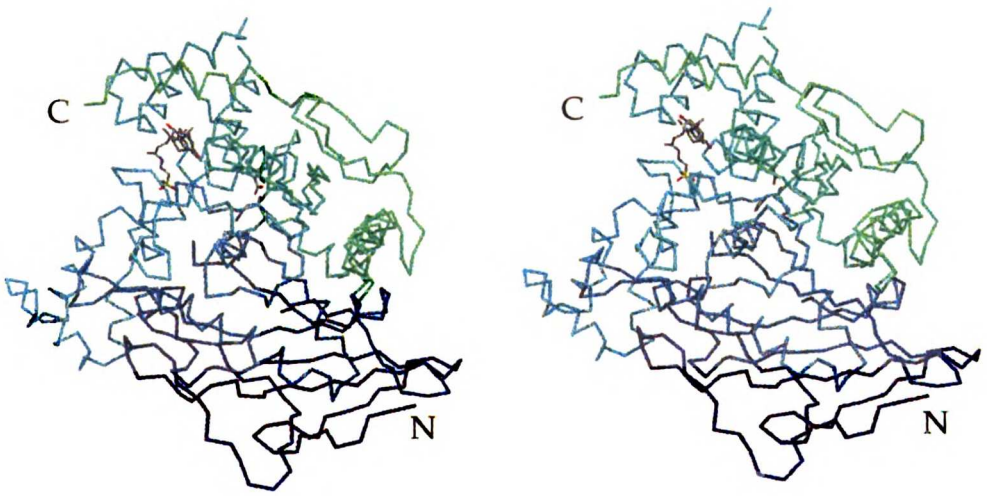

Figure 3.

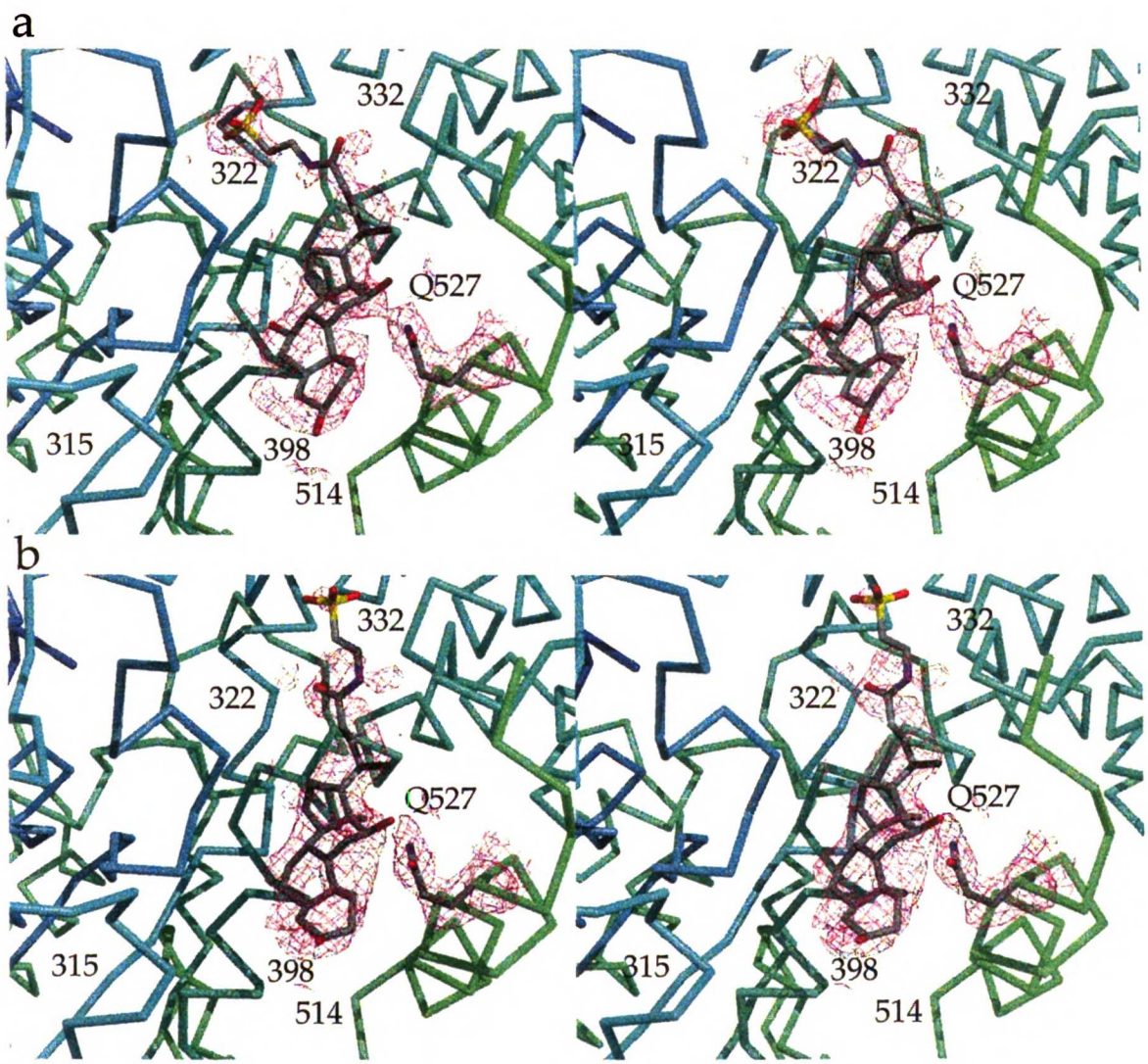
a
332
322
Q527
315
398
514
332
322
Q527
315
398
514
b
332
322
Q527
315
398
514
332
322
Q527
315
398
514

Figure 4.